

## Geologic and Structural Setting of Gold Mineralization in the Kirkland Lake-Larder Lake Gold Belt, Ontario

V. ISPOLATOV,<sup>†,\*</sup> B. LAFRANCE,

*Mineral Exploration Research Centre, Department of Earth Sciences, Laurentian University, Willet Green Miller Centre, 933 Ramsey Lake Rd., Sudbury, Ontario, Canada P3E 6B5*

B. DUBÉ,

*Geological Survey of Canada Quebec, 490 rue de la Couronne, Québec, Québec, Canada G1K 9A9*

R. CREASER,

*Department of Earth and Atmospheric Sciences, 1-26 Earth Sciences Building, University of Alberta, Edmonton, Alberta, Canada T6G 2E3*

AND M. HAMILTON

*Jack Satterley Geochronology Laboratory, University of Toronto, Toronto, Ontario, Canada M5S 3B1*

### Abstract

The Kirkland Lake-Larder Lake gold belt includes the giant Kirkland Lake and world-class Kerr-Addison-Chesterville gold deposits, along with several smaller deposits and occurrences. It corresponds to an east-trending band of Timiskaming clastic and volcanic rocks that unconformably overlie older volcanic assemblages in the southern Abitibi greenstone belt of the Archean Superior province. The gold belt is bounded to the south by the Larder Lake-Cadillac deformation zone, which roughly follows the contact between the younger Timiskaming rocks and the older volcanic units. Three generations of fabrics formed during post-Timiskaming regional deformation ( $D_2$ ,  $D_3$ , and  $D_4$ ) of the belt. North-south shortening during  $D_2$  produced a penetrative, generally east-striking, steeply dipping,  $S_2$  foliation, and an east-plunging,  $L_2$  stretching lineation.  $S_2$  is most intense within the syn- $D_2$  Larder Lake-Cadillac deformation zone and its northeast-trending splay, the Upper Canada deformation zone. The  $D_2$  structures are overprinted by a north-trending crenulation cleavage  $S_3$ , which formed during east-west  $D_3$  shortening across the belt. A northeast-trending regional  $S_4$  foliation associated with Z-shaped  $F_4$  folds and overprinting both  $S_2$  and  $S_3$  formed during northwest-southeast  $D_4$  shortening. Gold mineralization is localized along the Larder Lake-Cadillac deformation zone (Anoki and McBean deposits), the Upper Canada deformation zone (Upper Canada deposit), and the brittle Kirkland Lake fault and '04 Break (Kirkland Lake deposit). The Upper Canada, McBean, and Anoki deposits formed during  $D_2$ , and, along with Kerr-Addison-Chesterville, Omega, and Cheminis deposits, are probably related to a regionally extensive hydrothermal system associated with the Larder Lake-Cadillac deformation zone. The sulfide-poor gold- and telluride-bearing quartz veins of the Kirkland Lake deposit are interpreted to have been emplaced during  $D_4$ , synchronous with reverse-dextral movement along the ore-controlling brittle Kirkland Lake fault. The Kirkland Lake mineralization has a distinct metal signature ( $Te > Au$ , Mo, Pb, Ag, high Au/Ag, low As) and probably represents a separate hydrothermal system linked to a deep magmatic (alkalic) fluid source and unrelated to mineralization along the syn- $D_2$  deformation zones.

### Introduction

THE KIRKLAND LAKE-LARDER LAKE gold belt (Thomson, 1950; Fig. 1) broadly corresponds to the east-trending, 3- to 5-km-wide succession of Late Archean Timiskaming rocks bounded to the south by the Larder Lake-Cadillac deformation zone. The belt hosts the giant Kirkland Lake and world-class Kerr Addison-Chesterville gold deposits and several smaller deposits and occurrences (Table 1). Gold mineralization is spatially associated with the Larder Lake-Cadillac deformation zone (e.g., Kerr-Addison-Chesterville, Cheminis, Omega, and McBean deposits) and subordinate high-strain zones (e.g., Upper Canada deposit). The Kirkland Lake gold

deposit, the largest in the area, occurs along the more brittle Kirkland Lake fault ("Main Break;" Todd, 1928), which is located about 2 km north of the Larder Lake-Cadillac deformation zone.

This paper summarizes the results of a 2-year field-based project that combined district-scale geologic mapping with more detailed studies of structural geology and gold mineralization (see Ispolatov et al., 2005, for additional data and geologic maps). The work concentrated in two areas: in Teck Township, near the town of Kirkland Lake (Teck mapping area), and in Gauthier Township, 15 km east of Kirkland Lake (Gauthier mapping area; Figs. 1, 2, 3). The structural timing and style of gold mineralization of the Kirkland Lake deposit are described and compared to those of deposits associated with the Larder Lake-Cadillac deformation zone. Our findings indicate that gold deposits hosted by the Larder Lake-Cadillac

<sup>†</sup> Corresponding author: e-mail, vispolatov@gmail.com

\* Present address: Barrick Gold Corporation, 700-1055 W. Georgia St., Vancouver, British Columbia, Canada V6E 2Y2.

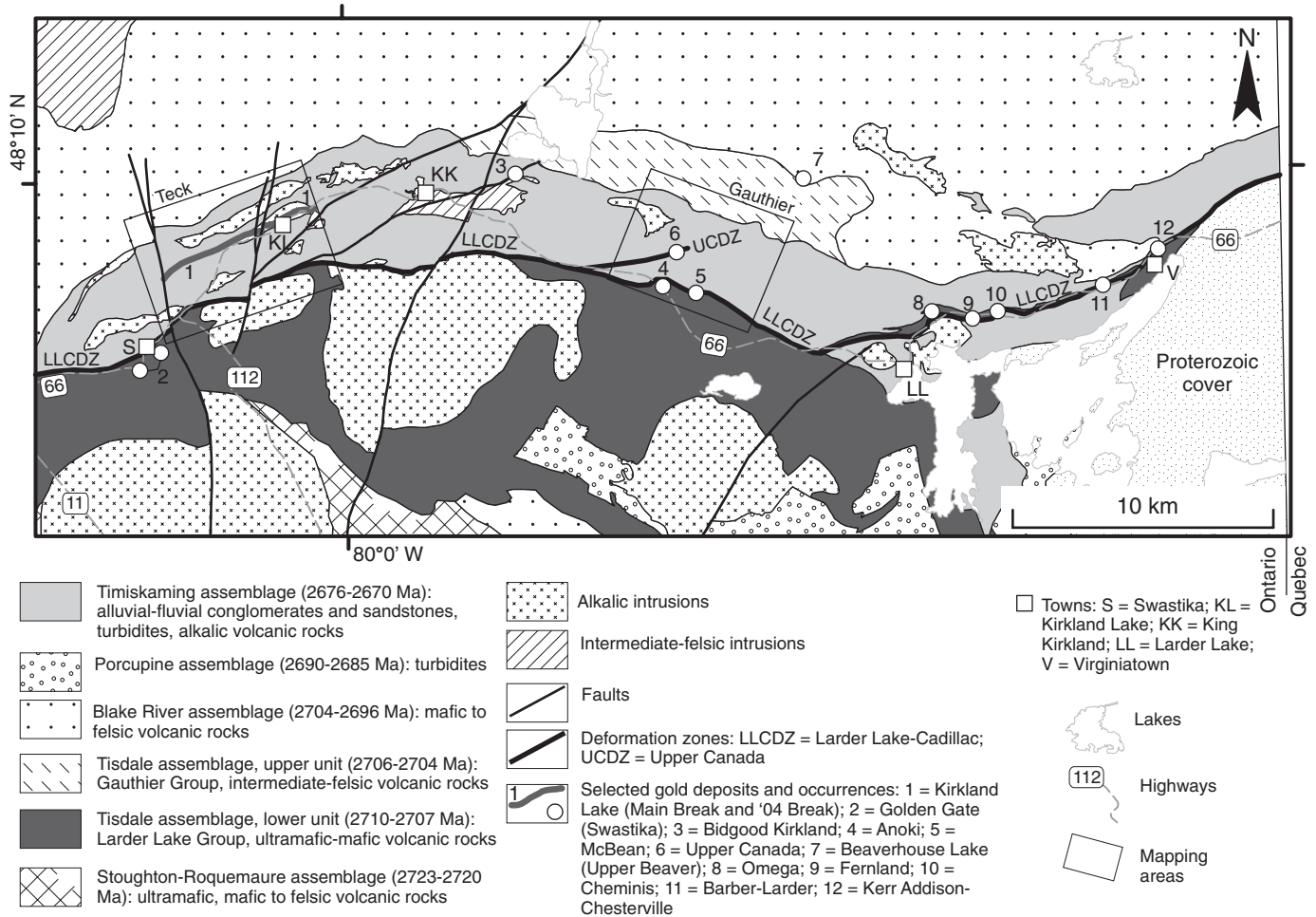


FIG. 1. Generalized map of the Kirkland Lake-Larder Lake gold belt, showing the location of Gauthier and Teck mapping areas. Compiled from Thomson (1941, 1945, 1950), Ayer et al. (2004, 2005), and Ispolatov and Lafrance (2005).

deformation zone and its splays are coeval with the earliest post-Timiskaming fabric-forming deformation event ( $D_2$ ). We interpret the giant Kirkland Lake gold deposit as a separate hydrothermal system that differs in style and geochemistry from gold deposits along the Larder Lake-Cadillac deformation zone and that formed during a later regional deformation event ( $D_4$ ).

### Regional Geology

The Kirkland Lake-Larder Lake gold belt is located in the southern Abitibi greenstone belt of the Archean Superior province (Card, 1990; Jackson and Fyon, 1991; Ayer et al., 2005). The Archean rocks in the area are metamorphosed to prehnite-pumpellyite up to greenschist grade (Jolly, 1978). They consist of older komatiitic, tholeiitic, and calc-alkaline volcanic rocks of the Tisdale (2710–2704 Ma) and Blake River (2704–2696 Ma) assemblages, which are unconformably overlain by clastic sedimentary and predominantly alkalic volcanic rocks of the Timiskaming assemblage (2676–2670 Ma; Fig. 1; Ayer et al., 2005). In the Gauthier mapping area, Timiskaming sedimentary rocks are represented by typically nongraded sandstones and conglomerates (unit 1, Fig. 2) and

well-graded sandstone-siltstone turbidites (unit 2, Fig. 2). Timiskaming volcanic rocks comprise intermingled lavas and tuffs, volcanoclastic breccias, sandstones, and conglomerates. U-Pb dating of detrital zircon from Timiskaming turbidites (this study) yielded a maximum depositional age of  $2677.7 \pm 3.1$  Ma; zircons from a Timiskaming feldspar-phyric lava flow returned an emplacement age of  $2669.6 \pm 1.4$  Ma (Fig. A1, Table A1). In the Teck mapping area (Fig. 3), Timiskaming rocks consist of steeply south dipping, south facing alkalic tuffs, conglomerates, and sandstones (max depositional U-Pb age of  $2680 \pm 3$  Ma; Corfu et al., 1991).

Felsic to intermediate (2695–2685 Ma) and alkalic (mainly syenitic; 2680–2672 Ma) stocks and dikes occur throughout the Kirkland Lake-Larder Lake gold belt (e.g., Ayer et al., 2005). The available radiometric ages of syenitic rocks (2680–2672 Ma) suggest that the alkalic plutonism in part overlapped with Timiskaming volcanism and sedimentation. Although Timiskaming sedimentary rocks are locally in erosional contacts with syenite stocks (Robert, 2001), most intrusions cut the Timiskaming stratified units. Most U-Pb ages are from plutons that lack direct intrusive contacts with the Timiskaming rocks (e.g., Wilkinson et al., 1999). These dates

TABLE 1. Historic Production and Regional Structural Setting for Selected Gold Deposits of the Kirkland Lake-Larder Lake Gold Belt

Deposit, mine	Regional structural setting	Mined ore (Mt)	Au production (t)	Au grade (g/t)	Years of production
Kerr-Addison-Chesterville deposit <sup>1</sup>					
Chesterville	LLCDZ	2.96	11.16	3.8	1930-1952
Kerr-Addison	LLCDZ	36.59	325.26	8.9	1911, 1938-1996
Total		39.55	336.43	8.5	
Barber-Larder					
Barber-Larder	LLCDZ	0.03	0.10	3.5	1988
Cheminis	LLCDZ	0.16	0.55	3.4	1991-1996
Omega	LLCDZ	1.47	6.66	4.6	1913, 1926-1928, 1936-1947
McBean	LLCDZ	0.51	1.43	2.8	1984-1986
Upper Canada	Upper Canada deformation zone	4.22	43.49	10.3	1938-1971
Kirkland Lake deposit <sup>2</sup>					
Toburn	Main Break	1.08	17.75	16.5	1917-1953 <sup>3</sup>
Sylvanite	Main Break	4.58	52.09	11.4	1927-1961
Wright Hargreaves	Main Break	9.01	149.96	16.6	1921-1965
Lake Shore	Main Break	15.61	267.58	17.1	1918-1965, 1982-1987, 1997-1998
Teck Hughes	Main Break	8.68	115.36	13.3	1917-1968
Kirkland Lake (Kirkland Minerals)	Main Break	2.85	36.48	12.8	1916-1960
Macassa	Main Break, '04 Break	7.15	109.65	15.4	1933-1999
Total		48.95	748.88 <sup>4</sup>	15.3	

Notes: Information from Ontario Ministry of Northern Development and Mines, Resident Geologist Program, posted in 2004; LLCDZ = Larder Lake-Cadillac deformation zone

<sup>1</sup> Includes Chesterville and Kerr-Addison mines, listed east to west

<sup>2</sup> Includes Toburn, Sylvanite, Wright Hargreaves, Lake Shore, Teck Hughes, Kirkland Lake and Macassa mines, listed east to west

<sup>3</sup> Intermittent production

<sup>4</sup> In addition to listed historic production, since 2002 Kirkland Lake Gold Inc. has been producing from the Macassa mine and Lake Shore ramp; the 2002 to 2004 production was 1.36 t Au (with an avg Au grade 9.6 g/t)

do not constrain the termination of alkalic magmatism, which may have continued after 2672 Ma, outlasting Timiskaming sedimentation.

The Kirkland Lake gold deposit is hosted by a three-phase alkalic intrusion consisting of, from oldest to youngest, mafic (augite) syenite, syenite, and syenite porphyry (e.g., Todd, 1928; Thomson et al., 1950; Figs. 3, 4). The intrusion is a 250- to 500-m-wide tabular, roughly concordant, west-plunging body, with thin discordant dike-like apophyses (Thomson et al., 1950; Ispolatov et al., 2005). The emplacement of the intrusion likely postdated tilting of host Timiskaming rocks to steep south dips (Thomson et al., 1950).

### Structural Geology

Three generations of structures, corresponding to three deformation events ( $D_2$ ,  $D_3$ , and  $D_4$ ) are recorded in rocks of the Timiskaming assemblage.  $D_1$  is an older deformation event that only affected pre-Timiskaming volcanic rocks (Wilkinson et al., 1999). Steeply dipping, southeast- to northeast-striking  $S_2$  is the main regional cleavage in the Gauthier mapping area (Fig. 5A). It is defined by banding and schistosity of metamorphic and hydrothermal chlorite, talc, white mica, and carbonate, and by flattened, elongate clasts in Timiskaming conglomerate and volcanoclastic rocks (Fig. 6A). The foliation is axial planar to rare, open to isoclinal, mesoscopic  $F_2$  folds in Timiskaming turbidites.  $S_2$  increases in intensity within the Larder Lake-Cadillac deformation zone, where it is parallel to bedding and lithologic contacts. The Larder Lake-Cadillac deformation zone is a first order, 400- to 600-m-wide,  $D_2$  high-strain zone, which encompasses several rock units and generally straddles the contact between

the Timiskaming belt and rocks of the Tisdale assemblage (Figs. 2, 3). A second, at least 300-m-wide, high-strain zone, the Upper Canada deformation zone, is exposed about 800 m north of the Larder Lake-Cadillac deformation zone (Fig. 2). It constitutes a second-order northeast-trending splay of the Larder Lake-Cadillac deformation zone; the two deformation zones reportedly merge under quaternary overburden west of the Gauthier mapping area (D.J. Toogood, unpub. report for Queenston Mining Inc., 1989, 57 p.).  $S_2$  contains a strong  $L_2$  lineation, which plunges 35° to 60° E (Fig. 5C) and is defined by elongate sericite-chlorite aggregates and stretched clasts and varioles (Fig. 6B). Southeast-plunging Z-shaped, asymmetric drag folds, pebbles with asymmetrical strain shadows (Fig. 7), and offset quartz veins indicate oblique reverse-dextral slip in the direction of  $L_2$  for the Larder Lake-Cadillac deformation zone. In the Teck mapping area,  $S_2$  (Fig. 5B) and  $L_2$  occur only within the 500- to 600-m-wide Larder Lake-Cadillac deformation zone; that is, they are not observed north of the deformation zone.

A second foliation,  $S_3$ , overprints  $S_2$  on several outcrops both inside and outside of the deformation zones. It is best developed in the Upper Canada deformation zone.  $S_3$  is a steeply dipping, north- (rarely, west-northwest)-trending, differentiated crenulation cleavage (Figs. 5D, 6C), which is axial planar to open to tight symmetrical folds. It is defined by darker, sericite- and chlorite-rich domains (0.5–3 mm wide) alternating with wider (3–10 mm) feldspar-carbonate-quartz domains in which  $S_2$  is finely crenulated (Fig. 6C).

$S_2$  and  $S_3$  are overprinted by a steeply dipping regional cleavage,  $S_4$ , which is axial planar to outcrop-scale Z-shaped  $F_4$  folds.  $S_4$  occurs in all rock units both within and outside the

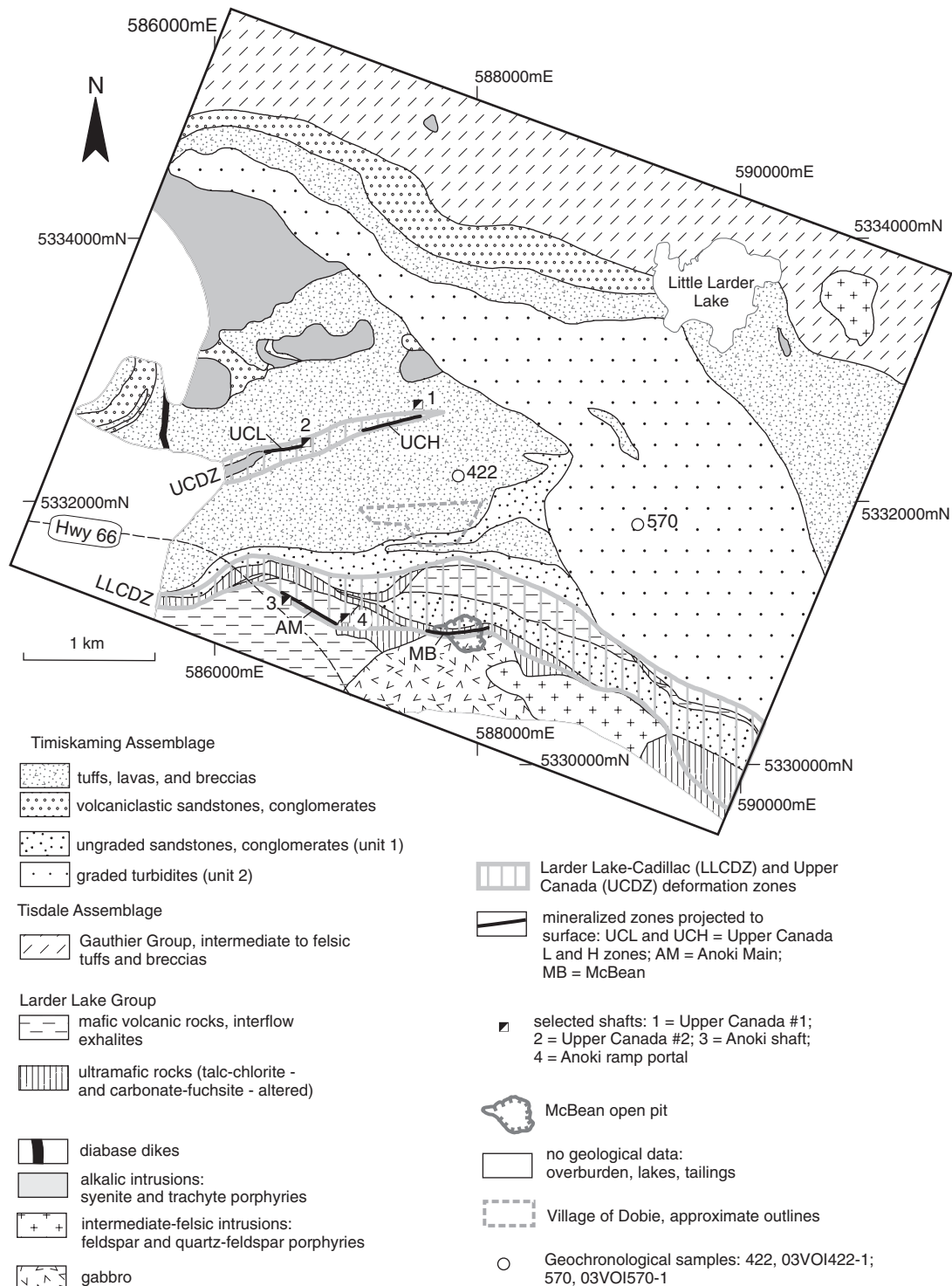


FIG. 2. Geology of the Gauthier mapping area. Modified from Ispolatov and Lafrance (2005) and based on new mapping by V. Ispolatov and B. Lafrance, data from Thomson and Griffis (1941), and unpublished data of Queenston Mining Inc. Coordinates are UTM zone 17 NAD 83.

Larder Lake-Cadillac deformation zone. In the Gauthier mapping area,  $S_4$  is a northeast-striking ( $060^{\circ}$ – $085^{\circ}$ ) differentiated crenulation cleavage (Figs. 5E, 6D). In the Teck mapping area,  $S_4$  strikes northeast ( $040^{\circ}$ – $065^{\circ}$ ; Fig. 5F) and is represented by a disjunctive and weak crenulation cleavage and

by the preferred orientation and weak flattening of clasts in Timiskaming conglomerates.

The Kirkland Lake gold deposit is associated with the brittle Kirkland Lake fault, also known as the Main Break (Todd, 1928; Thomson, 1950; Charlewood, 1964; Fig. 3). In the

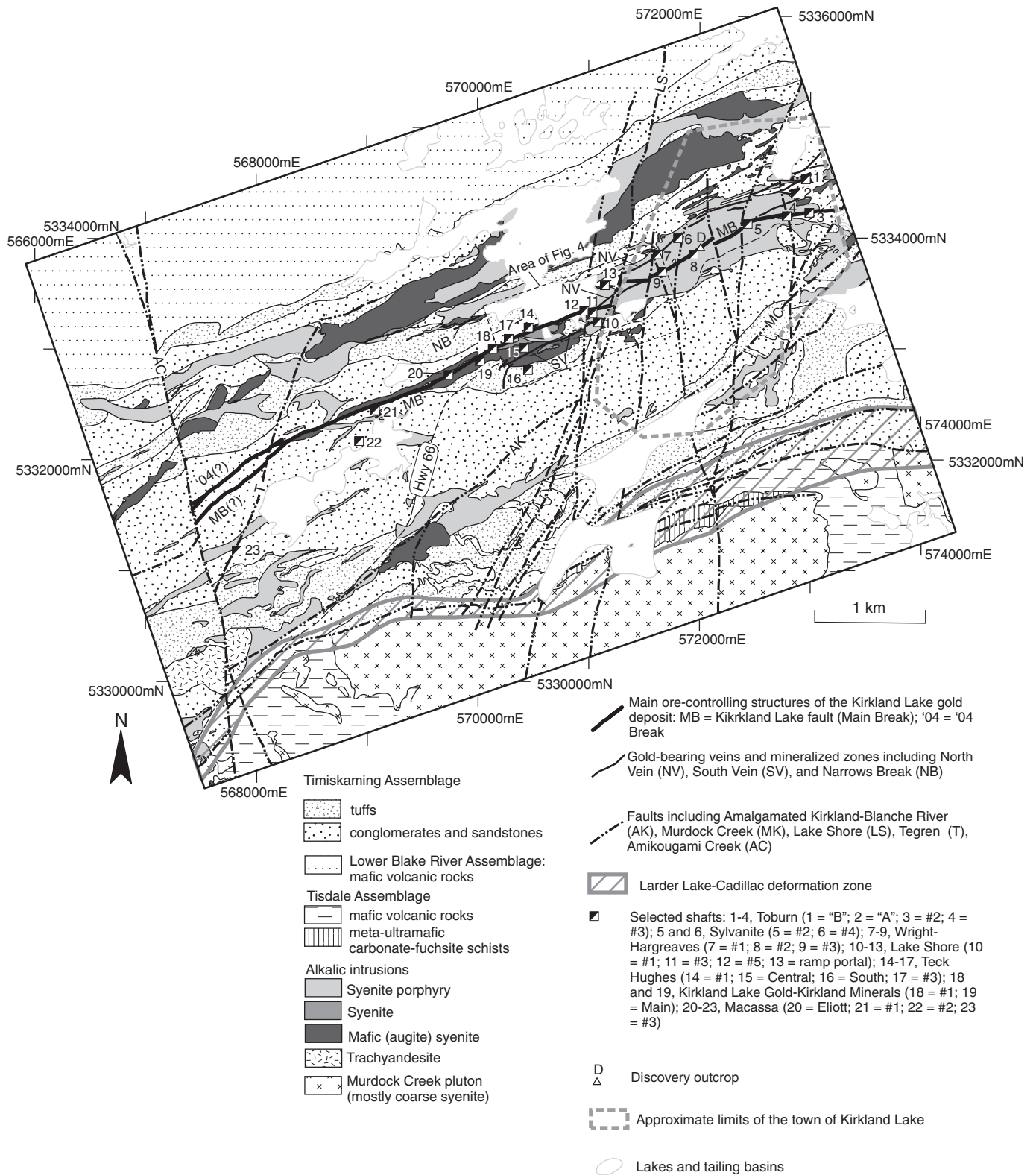


FIG. 3. Geology of the Teck mapping area. Modified from Ispolatov (2005) and based on data from Todd (1928), Thomson (1945), new mapping by V. Ispolatov, and unpublished data of Kirkland Lake Gold Inc. Coordinates are UTM zone 17 NAD 83.

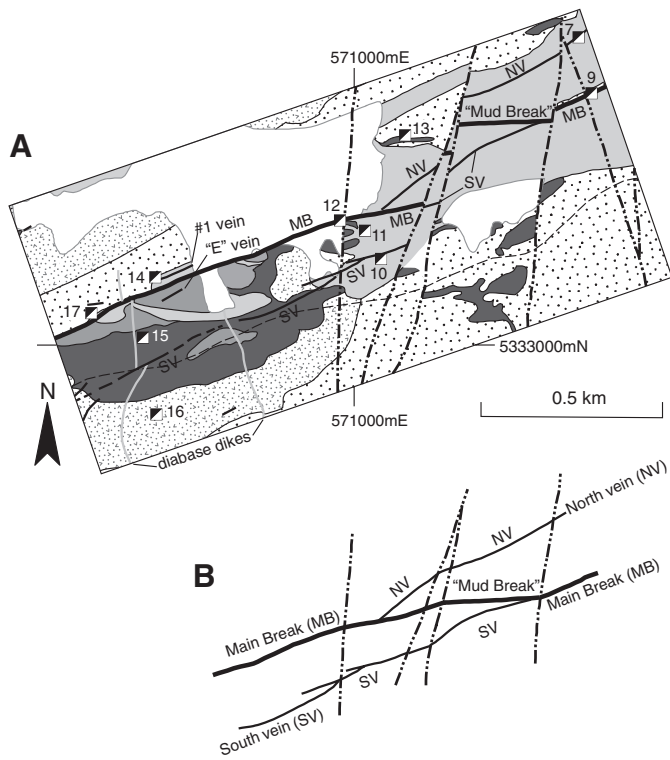


FIG. 4. A. Geology of the central part of the Kirkland Lake gold deposit (parts of Teck Hughes, Lake Shore, and Wright-Hargreaves properties), showing location of Teck Hughes 1 and "E" veins, and the "Mud Break." Same legend as Figure. 3. Based on Todd (1928), Thomson (1945), and Ispolatov (2005). B. Ore-hosting structures reconstructed "without" postore fault displacement. Coordinates are UTM zone 17 NAD 83.

eastern and central parts of the deposit (Toburn, Sylvanite, Wright-Hargreaves, Lake Shore, and Teck Hughes mines), mineralization also occurs along two approximately parallel splays of the Main Break, called the North and South vein structures (Figs. 3, 4). The Main Break strikes northeast ( $060^{\circ}$ – $080^{\circ}$ ), dips steeply south ( $60^{\circ}$ – $85^{\circ}$ ), and was traced continuously at surface and underground over a distance of about 4,800 m, from the Toburn mine to the eastern part of the Macassa mine (Fig. 3; Charlewood, 1964). Near Macassa shafts 1 and 2, at depths of 1,200 to 1,400 m, the Main Break splits into north and south branches, and the more persistent north branch connects to another fault, the '04 Break, via several minor faults (Charlewood, 1964; Watson and Kerrich, 1983; Watson, 1984). In this area, at a depth of about 1,400 m, the '04 Break is approximately parallel to the Main Break, it is located 140 m to the north, strikes about  $060^{\circ}$  and dips  $60^{\circ}$  to  $65^{\circ}$  south. Farther west, the '04 Break becomes the main ore-controlling structure. Drifts in the western part of Macassa mine systematically follow the '04 Break: it is traced underground (1,100–2,100 m below surface) for about 1,700 m from Macassa shafts 1 and 2 to the Amikougami Creek fault. At surface, two northeast-striking ( $050^{\circ}$ – $060^{\circ}$ ), nearly parallel faults, 100 to 120 m apart, have been mapped west of Macassa shaft 2 (Fig. 3). The north and south faults are interpreted as the '04 Break and Main Break, respectively (Ispolatov et al., 2005).

Underground at the Macassa mine, the Main Break and the '04 Break are represented by single or multiple (branching),

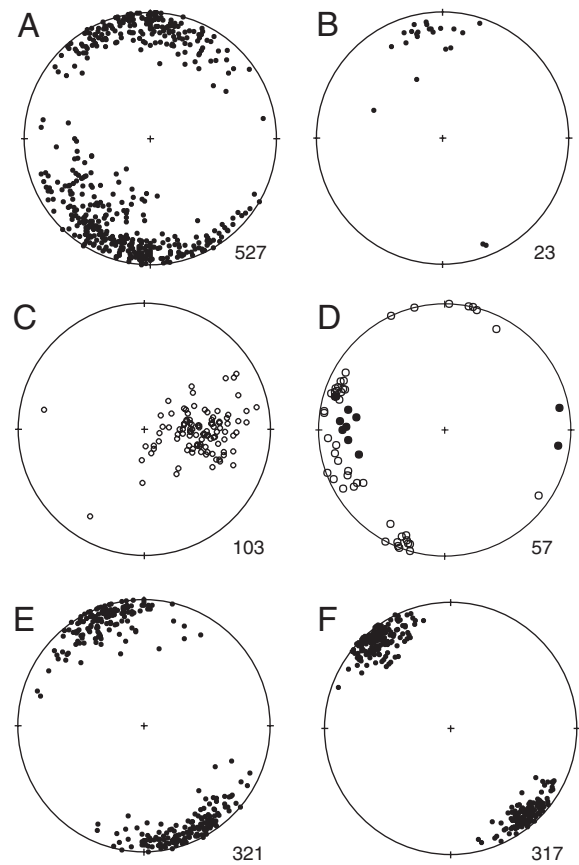


FIG. 5. Equal-area lower hemisphere stereonet projections of deformational fabrics, with numbers of measurements. A and B. Poles to  $S_2$  in Gauthier and Teck mapping areas, respectively. C.  $L_2$  (Gauthier mapping area). D. Poles to  $S_3$ , Gauthier mapping area (open circles, within Upper Canada deformation zone; filled circles, all other locations). E and F. Poles to  $S_4$  in Gauthier and Teck mapping areas, respectively. (Note:  $S_2$  and  $S_4$  data from detailed mapping of the Upper Canada stripped outcrops are excluded and shown separately in Fig. 15).

5- to 10-cm-wide, chloritic slips or gouge bands (Fig. 8A), typically surrounded by wider (0.5–2.5 m) envelopes of carbonatized fine-grained, grayish light brown to reddish brown cataclasite. Macroscopically, the cataclasite is largely aphanitic, with rare 1- to 2-mm feldspar fragments. The cataclasite commonly shows banded texture defined by reddish brown discontinuous bands (1–3 cm wide) separated by a darker chloritized matrix. Breccia, consisting of 1- to 3-cm clasts occurs locally. Weak striations on chloritic slip planes plunge steeply (rake  $60^{\circ}$ – $90^{\circ}$  east and west) and shallowly (rake  $0^{\circ}$ – $30^{\circ}$  west and, more rarely, east) indicating both dip-slip and strike-slip movements along the faults. At one stope along the '04 Break at the Macassa mine (4528 MCF), a weakly developed foliation, defined by the alignment of clasts and diffuse compositional banding in fault breccia, dips more steeply to the south ( $80^{\circ}$ – $85^{\circ}$ ) than the Break ( $55^{\circ}$ – $60^{\circ}$ ). Such an orientation suggests a reverse (south over north) movement along the fault at some point in its history.

In surface exposures on the former Lake Shore property (east of the shaft 5), the Main Break comprises branching northeast-striking ( $060^{\circ}$ – $075^{\circ}$ ), south-dipping ( $75^{\circ}$ – $80^{\circ}$ ), 10- to 25-cm-wide shears, consisting largely of hydrothermal

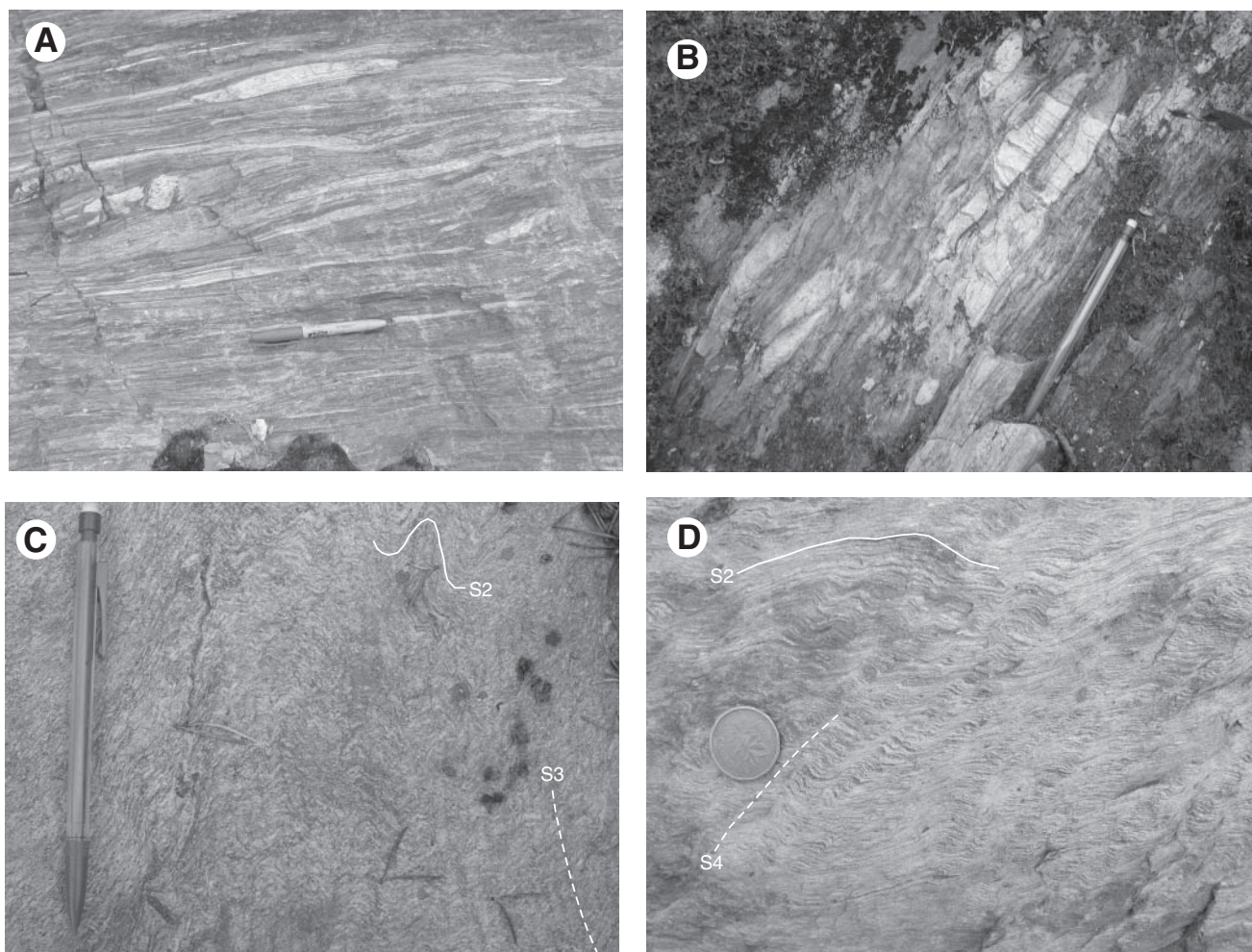


FIG. 6. Field photographs of deformation fabrics (Gauthier mapping area). A.  $S_2$  defined by flattened clasts in Timiskaming conglomerates, plan view, facing north. B.  $L_2$  defined by eastward-plunging stretched clasts in Timiskaming volcanoclastic breccias, cross-section view, facing south. C. Crenulation  $S_3$  cleavage overprinting  $S_2$  in a feldspar-phyric syenite porphyry, plan view, facing north. D. Crenulation  $S_4$  cleavage overprinting  $S_2$  in a strongly altered felsic dike. Plan view, facing north, coin diameter is 2 cm.

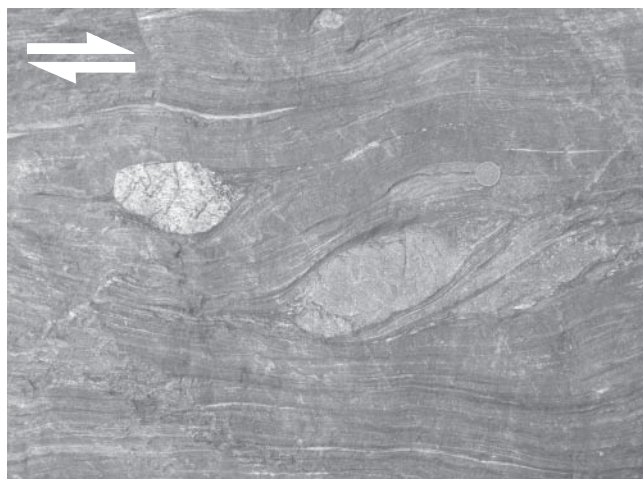


FIG. 7. Asymmetric pressure shadows around granitic clasts indicating reverse-dextral slip parallel to  $L_2$  lineation. Timiskaming conglomerates in the northern wall of the McBean open pit, outcrop surface is approximately parallel to  $L_2$  lineation. Coin diameter is 2 cm.

sericite. The shears show an internal S-type foliation oriented oblique to their boundaries, both in plan and cross-section view. In plan view, the foliation is oriented at  $15^\circ$  to  $20^\circ$  counterclockwise of the shear boundaries; in cross-section view, the foliation dips more steeply than the shears (Fig. 8B, C). This indicates a reverse-dextral (south side up and to the west) slip along the Main Break.

The east-striking segment of the Main Break between the North and South veins, informally known as the "Mud Break," is exposed farther east, at the west border of the former Wright-Hargreaves property (Fig. 4). An approximately 20-m-wide, east-striking, low-grade ( $Au \leq 3-4$  g/t) mineralized zone comprising weak stockwork and pyrite-bearing (2–10%) replacement is associated with the structure. The Mud Break is a 3- to 4-m-wide high-strain zone consisting of strongly sericitized and foliated syenite porphyry (Fig. 8D, E). The sericite alteration is associated with small mineralized quartz veinlets (Fig. 8F). The foliation, which formed synchronously with or after sericitization, strikes east, parallel to the overall orientation of the Mud Break. The relative timing

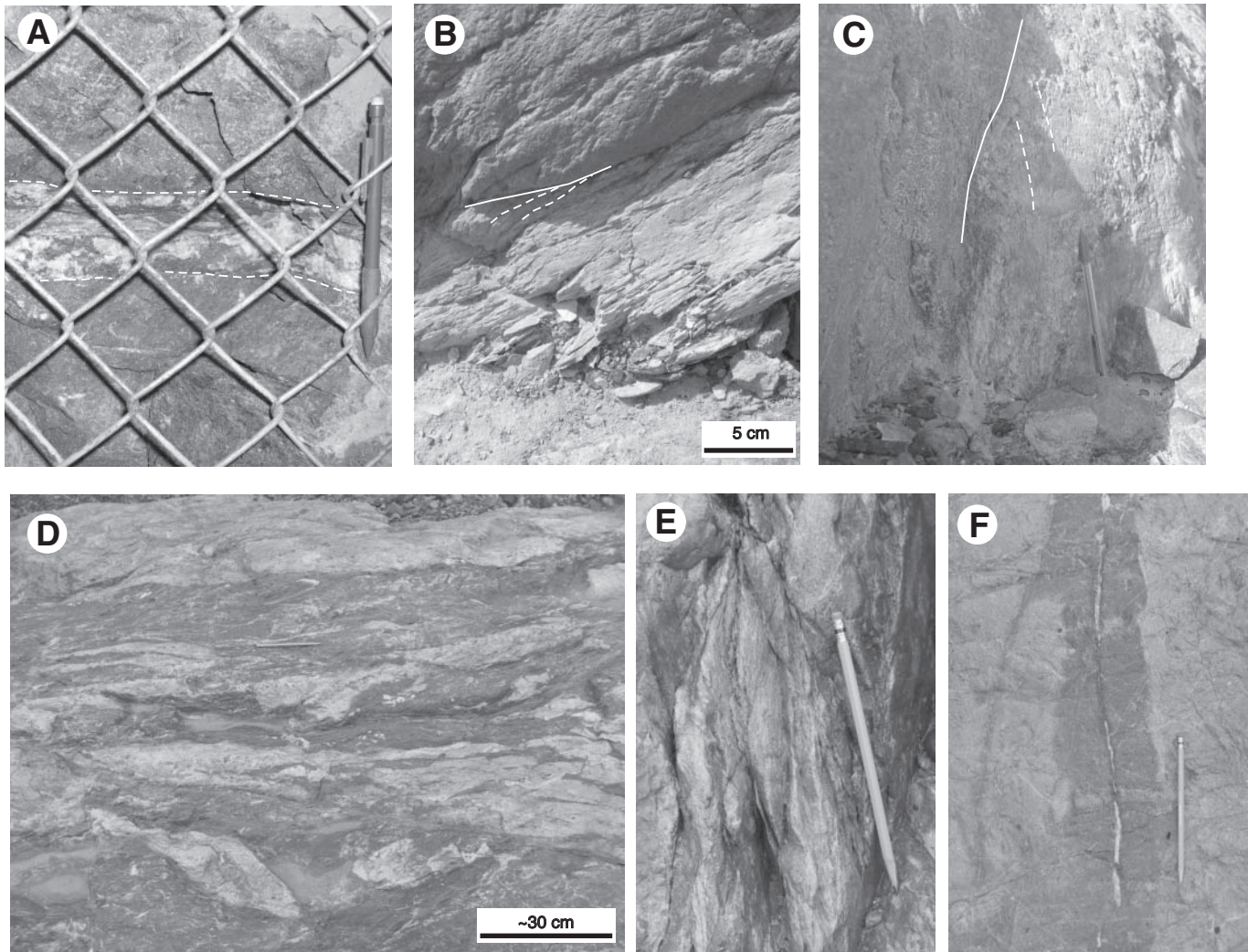


FIG. 8. A. Chloritic slip along the Main Break with late (postore) carbonate-quartz veining; back of a drift at the 4500-ft level of the Macassa mine. B, C. Sericitic foliation along the Main Break east of the former Lake Shore shaft 5 (B, plan view facing approximately south; C, cross section view looking west). Foliation (highlighted by dashed lines) is oriented obliquely to fault walls (highlighted by solid lines), which is consistent with oblique reverse-dextral sense of movement. D. Outcrop view of the "Mud Break;" darker bands correspond to sericite-rich foliated domains. E. Close-up cross-sectional view of a foliated sericite-rich band within the "Mud Break." F. Undeformed symmetrical sericitization halo around a quartz veinlet ("Mud Break" mineralized zone).

of movements on the Main Break and the '04 Break with respect to deformational events and gold mineralization is discussed later.

### Gold Mineralization

#### *Anoki and McBean deposits (Larder Lake-Cadillac deformation zone)*

Gold mineralization along the Larder Lake-Cadillac deformation zone is exemplified by the Anoki and McBean deposits. The main mineralized zone of the Anoki deposit is a tabular (~60 m width  $\times$  ~450 m length, Fig. 9) zone, containing measured and indicated resources of 522,300 metric tonnes (t) with a grade of 5.7 g/t Au (2.98 t Au) and inferred resources of 35,800 t with a grade of 5.7 g/t (0.2 t Au; Queenston Mining Inc., Annual Report, 2003, 24 p.). The

mineralized zone is hosted in pillowed to massive Fe tholeiitic basalts of the Larder Lake Group (Tisdale assemblage) and is parallel to lithologic contacts in the volcanic sequence. It dips steeply ( $60^{\circ}$ – $65^{\circ}$ ) north, strikes west-northwest, and plunges approximately  $30^{\circ}$  to the east (Fig. 9). A distinctive magnetite-rich, high Fe/Mg [molar Fe/(Fe + Mg) = 0.65] flow unit constitutes the protolith for the replacement-style mineralization. At the flanks of the mineralized zone, where bulk alteration is relatively weak, well-defined sulfidation (pyrite) halos occur around thin quartz stringers (Fig. 10A). Within the mineralized zone, the rocks are strongly altered, massive, and are light gray to brownish light gray (Fig. 10B). They consist of euhedral to subhedral hydrothermal albite, carbonate, up to 15 vol percent coarse (1–5 mm) pyrite, with minor quartz and sericite. Few quartz and quartz-carbonate veinlets (0.3–1 cm thick) are present. Reflected light

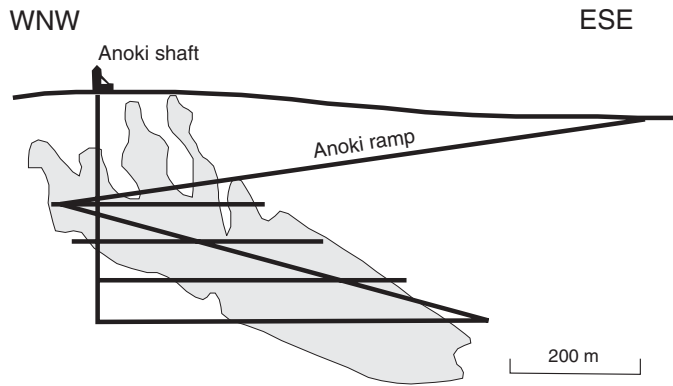


FIG. 9. Vertical longitudinal section of the Anoki Main zone (modified from Queenston Mining Inc., Annual Report, 1996, 14 p.). The zone dips 60° to 65° north, away from the viewer.

petrography and SEM imaging show that gold occurs as very small (0.002–0.05 mm) inclusions in pyrite together with larger inclusions of chalcopyrite, sphalerite, and galena. The mineralization is characterized by elevated Cu and As and 5 to 7 wt percent S.

The McBean deposit is hosted by a band of metamorphosed, hydrothermally altered, and highly strained ultramafic rocks along the southern margin of the Larder Lake-Cadillac deformation zone. The ultramafic rocks are flanked by gabbros and basalts to the south and by Timiskaming conglomerate and sandstone to the north. Numerous feldspar porphyry and syenite dikes intrude the ultramafic rocks (Bell, 1987). The deposit is spatially associated with a bend along the Larder Lake-Cadillac deformation zone; the attitude of

the host rocks changes from southeast- to east-striking with a decrease in dip from 75°–80° to 60° (south; Fig. 11). Mineralization occurs over a strike length of about 600 m, is roughly parallel to lithologic contacts and S<sub>2</sub> foliation, and plunges approximately 50° east. Measured and indicated resources of the McBean deposit are 835,520 t with a grade of 5.1 g/t (4.26 t Au) and inferred resources are 1,835,230 t with a grade of 6.5 g/t (11.93 t Au; Queenston Mining Inc., Annual Report, 2003, 24 p.). Near-surface mineralization, which was mined as an open-pit operation during the 1980s, consists of low-grade zones in altered syenite dikes. Fine-grained gold is associated with pyrite that formed by sulfidation of primary magnetite in the dikes (Bell, 1987). At deeper levels (≥300 m below surface) explored by drilling, gold occurs in zones of quartz veins hosted by ultramafic carbonate-fuchsite schists (“green carbonate ore”) and in volumetrically subordinate quartz-carbonate-sericite-altered aphyric dikes with disseminated pyrite and small quartz veinlets. The grades in these deep zones are typically higher than those in the pit, with visible gold commonly present in the quartz veins (D. Alexander, Queenston Mining Inc., pers. commun., 2003). In carbonate-fuchsite schists enveloping the gold-bearing zones, S<sub>2</sub> is defined by intercalated carbonate-, fuchsite-, and chlorite-rich bands and is overprinted by a discrete S<sub>4</sub> crenulation cleavage.

#### Upper Canada mine (Upper Canada deformation zone)

The Upper Canada mine operated from 1938 to 1971 and produced 43.49 t of gold at an average grade of 10.3 g/t (Table 1) and an Au/Ag ratio of 2.22 (Tully, 1963). The mine is situated along the northeast-striking Upper Canada deformation zone (“Upper Canada Break;” Tully, 1963). Most of the ore was mined from the L zone, which is located at the contact or within 150 m of the contact between an east-plunging feldspar-phyric syenite porphyry stock and Timiskaming volcanic rocks. The L zone has been mined and explored to a depth of 2,015 m (Tully, 1963). It strikes parallel to the host deformation zone (~070°–075°), dips steeply to vertically, and plunges 40° to 60° to the east (Fig. 12).

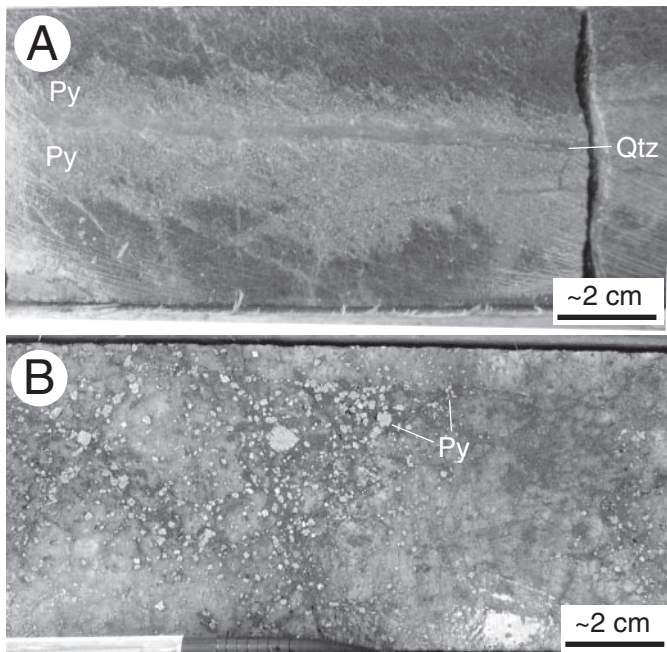


FIG. 10. Anoki Main zone mineralization. A. Drill core photograph of sulfidation (pyrite, Py) halo around a thin quartz veinlet (Qtz) at the margin of the mineralized zone. B. Drill core photograph of strongly altered basalt with pyrite (Py) cubes.

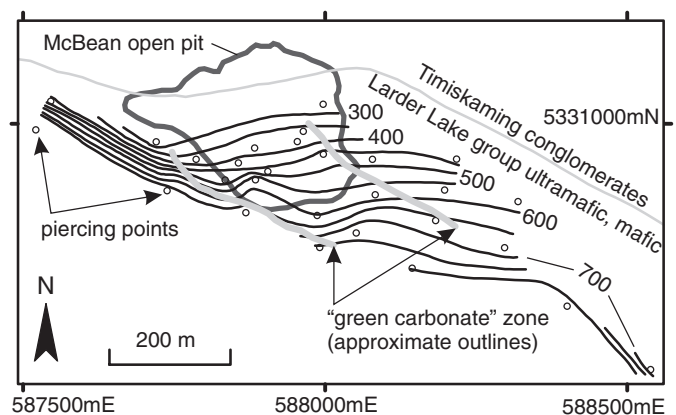


FIG. 11. Structural contours (depth from surface in meters) of the southern contact of the Timiskaming conglomerate-sandstone unit at the McBean deposit (based on unpublished drilling data of Queenston Mining Inc.). The mineralized “green carbonate” zone is located in the structurally overlying volcanic rocks of the Larder Lake Group. Coordinates are UTM zone 17 NAD 83.

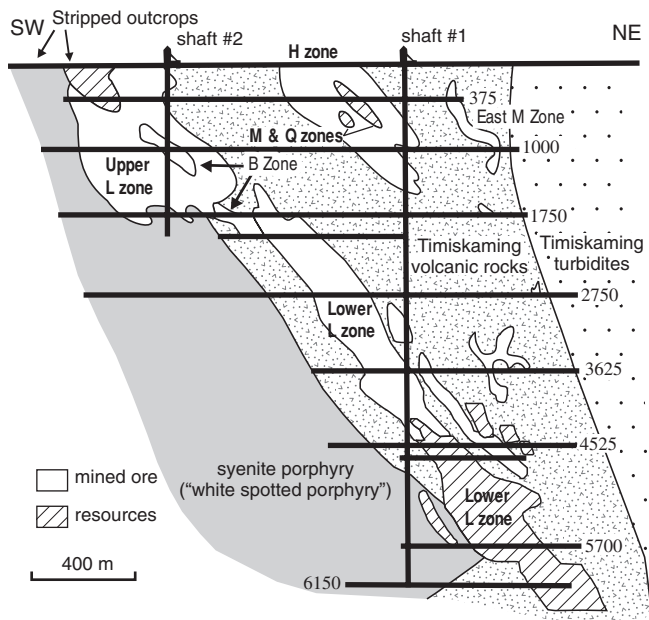


FIG. 12. Upper Canada mine, vertical longitudinal section, looking north-west (modified from Stevenson et al., 1995, and Queenston Mining Inc., Annual Report, 1996, 14 p.).

The westernmost part of the L zone is exposed at surface on several stripped outcrops west of shaft 2, where the syenite porphyry forms a wedge-shaped, eastward-tapering body in contact with tuffs and tuff breccias (Figs. 13, 14). The deformed tuffs are aphanitic or contain up to 5 to 10 vol percent relict feldspar grains (0.5–2 mm) and are altered to quartz, sericite, and carbonate. Tuff breccias consist of angular (1–5 to 7–10 cm) lithic (volcanic) clasts enclosed in a strongly tourmalinized matrix. The syenite porphyry contains 20 to 40 vol percent ovoid feldspar phenocrysts (1–3 mm) within an altered (quartz-sericite,  $\pm$ carbonate) matrix. Disseminated fine-grained pyrite occurs throughout the rocks without apparent correlation between pyrite content and gold grades. The boundaries of the L zone are assay defined and correspond to gold grades  $\geq 1$  g/t (Fig. 14). The westernmost

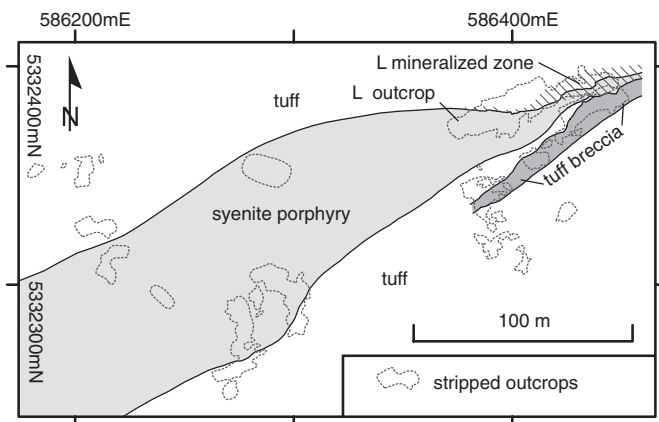


FIG. 13. Location map of stripped outcrops west of Upper Canada shaft 2, showing the distribution of major rock types. (Outcrop outlines modified from D.J. Toogood, unpub. report for Queenston Mining Inc., 1989, 57 p.). Coordinates are UTM zone 17 NAD 83.

exposed extent of the L zone is confined to a 0.3- to 2.0-m-wide, sharply bounded band of carbonate-rich (8–15 wt %  $\text{CO}_2$ ) quartz-sericite schist at the north contact of the syenite porphyry stock. The grades are generally lower to the east where the zone widens (up to 8–10 m) and includes parts of the porphyry and host tuffs.

Three penetrative foliations are observed on the stripped outcrops (D.J. Toogood, unpub. report for Queenston Mining Inc., 1989, 57 p.).  $S_2$  is a steeply dipping, northeast-striking ( $065^\circ$ – $085^\circ$ ), differentiated cleavage defined by domains rich in carbonate and quartz, alternating with thinner sericite-rich domains that contain trails of fine-grained anhedral pyrite (0.1–0.2 mm) and titanite (Figs. 15A, 16A). It is also marked by the preferred orientation of flattened and recrystallized feldspar phenocrysts in syenite porphyries and by flattened clasts in tuff breccias.  $S_2$  is overprinted by  $S_3$ , which forms a steeply dipping, typically north-striking ( $340^\circ$ – $020^\circ$ ), differentiated crenulation cleavage, defined by 1- to 2-mm-wide sericite-rich folia containing minor pyrite, titanite, and, locally, tourmaline (Figs. 5D, 6C).  $S_3$  cleavage is oriented at a high angle ( $60^\circ$ – $90^\circ$ ) to  $S_2$  and is axial planar to open folds defined by folded  $S_2$ . Both  $S_2$  and  $S_3$  are overprinted by and locally transposed parallel to a steeply dipping, northeast-trending ( $065^\circ$ – $080^\circ$ )  $S_4$  cleavage (Figs. 15B, 16B).  $S_4$  is a differentiated cleavage defined by discrete sericite- and pyrite-rich cleavage planes, transposed  $S_2$  and probably  $S_3$ , and quartz fibers in fringes around pyrite grains. The occurrence of pyrite clusters along  $S_4$  planes suggest that pyrite was either deposited or redistributed during  $D_4$ . Northeast-plunging  $F_4$  folds defined by folded  $S_2$  are generally Z shaped (Figs. 15B, 16A). Barren, 2- to 10-cm-thick, quartz  $\pm$  albite-carbonate veins are strongly folded parallel to  $S_2$  and  $S_4$ . A later similar set of steeply dipping, north-striking, quartz  $\pm$  albite-carbonate veins cut across all deformational fabrics in the rocks.

In cut slabs and thin sections, gold (grains of 0.02–0.1 to 0.5 mm) occurs in thin (1–3 mm), pervasive, carbonate-rich, quartz-carbonate veinlets, which are parallel to  $S_2$  and folded about Z-shaped  $F_4$  folds (Fig. 17). Gold-bearing veinlets show lower  $D_2$  strain than some quartz-rich,  $S_2$  parallel bands in the host schist. In the veinlets, gold is sited in apparent textural equilibrium with carbonate and quartz. Tennantite [(Cu,Fe) $_{12}$ As $_4$ S $_{13}$ ], minor chalcopyrite, and rarely pyrite, scheelite, and arsenopyrite are associated with gold (Fig. 17B). In addition to these minerals, Tully (1963) reported the presence of molybdenite, galena, and altaite in the Upper Canada ores.

#### Kirkland Lake gold deposit (Main Break and '04 Break)

Gold production in Kirkland Lake began in 1915 (Todd, 1928). Through the 20<sup>th</sup> century, the Macassa, Kirkland Lake Gold (later Kirkland Minerals), Teck-Hughes, Lake Shore, Wright-Hargreaves, Sylvanite, and Toburn mines, which operated on the same giant Kirkland Lake gold deposit, collectively produced 748 t of gold from 48.9 Mt of ore with an average grade of 15.3 g/t (see Table 1). Underground workings extend to about 2.5 km below the surface, and mineralization remains open to depth (Charlewood, 1964). The production-based (1913–1962) Au/Ag ratio averaged 5.4 for the entire deposit, with the highest (9.0) at Kirkland Lake Gold (Kirkland Minerals) and the lowest (4.2) at Toburn (Charlewood, 1964). At present, Kirkland Lake Gold Inc. owns Macassa, Kirkland

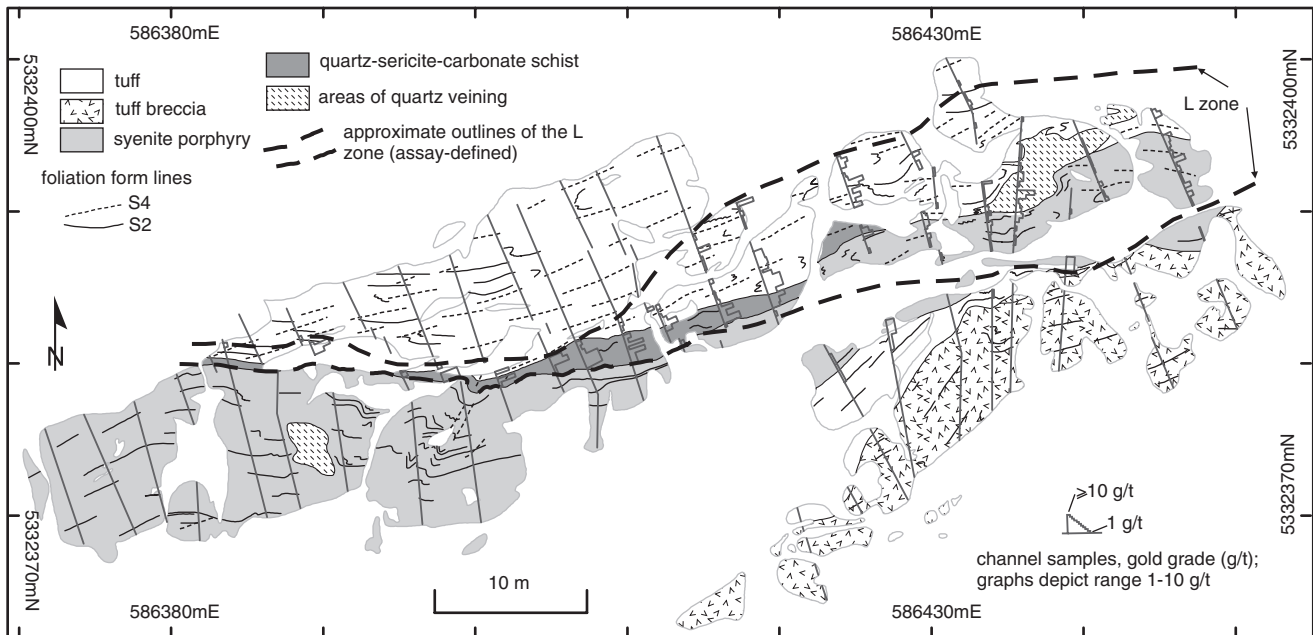


FIG. 14. Geologic map of the L stripped outcrop (outcrop outlines and gold grade graphs are from D.J. Toogood, unpub. report for Queenston Mining Inc., 1989, 57 p.). Graphs depict gold grades from 1 to greater than 10 g/t (i.e., gold grades >10 g/t are not differentiated). Coordinates are UTM zone 17 NAD 83.

Minerals, Teck-Hughes, Lake Shore, and Wright-Hargreaves mines and produces gold from the Macassa 2 and 3 shafts and Lake Shore ramp. As of 2005, reserves (proven + probable) and resources comprised, respectively, 28.9 and 22.4 t Au (avg grades of 15.8 g/t and 12.7 g/t; Heffernan, 2005).

Gold mineralization at the Kirkland Lake deposit is localized along the northeast-striking, steeply south dipping Kirkland Lake fault (the Main Break) and the '04 Break, as well as along several splays of these faults (e.g., North and South vein structures, Figs. 3, 4; Todd, 1928; Thomson et al., 1950; Charlewood, 1964; Watson and Kerrich, 1983; Watson, 1984; Still, 2001). Ore-controlling faults cut and displace a composite alkalic intrusion consisting of mafic syenite, syenite, and syenite porphyry (Hopkins, 1940; Thomson et al., 1950). Typical mineralization consists of relatively sulfide poor quartz veins hosted mainly by alkalic intrusive rocks; few ore bodies occur in Timiskaming tuffs, sandstones, and conglomerates.

Economic grades are related to gold contained in quartz veins, rather than in altered host rocks. In the veins, native gold is associated with telluride minerals, such as altaite, calaverite, petzite, and coloradoite (Todd, 1928; Thomson et al., 1950). Other metallic minerals include pyrite, chalcopyrite, molybdenite, minor sphalerite, and very rare arsenopyrite (Thomson et al., 1950). The ore-controlling faults and auriferous veins are cut by Paleoproterozoic Matachewan diabase dikes and are offset by postore faults, including the Amikougami Creek, Tegren, Lake Shore, Murdock Creek, and Sylvania faults (e.g., Hopkins, 1940; Thomson et al., 1950). No economic ore has been found to date west of the Amikougami Creek fault. The description of structures and gold mineralization below focuses largely on the '04 Break because it is the main ore-controlling structure at the currently active Macassa mine.

**Gold-bearing veins:** Gold mineralization at the Macassa mine is associated with quartz veins, and, locally, with zones of discontinuous auriferous quartz lenses and pods in inter-fingering syenitic intrusions and tuffs (Watson, 1984). The latter mineralization style, informally termed "breccia ore" (Watson, 1984), is presently inaccessible and is not discussed in this paper. Principal types of gold-bearing quartz veins at Macassa include veins hosted by or localized in the immediate proximity to the Main Break and the '04 Break ("break ore"), and footwall and hanging-wall veins ("vein ore;" Watson, 1984; Still, 2001). In addition to veins exposed underground at the Macassa mine, several veins that are exposed at surface are also described. These include veins hosted by the Main Break at the Discovery outcrop on the former Wright-Hargreaves property and east of the former Lake Shore shaft 5, and the Teck-Hughes 1 vein (Fig. 4), which is hosted by a north splay of the Main Break (Todd, 1928). Due to their

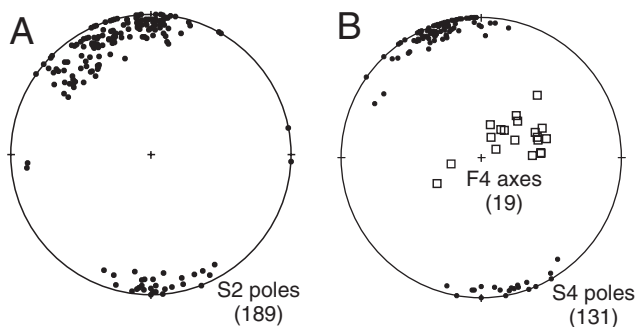


FIG. 15. Equal-area lower hemisphere projections of deformational fabrics from the Upper Canada L stripped outcrop (numbers of measurements in parentheses). A. Poles to S<sub>2</sub>. B. F<sub>4</sub> fold axes (folded S<sub>2</sub>) and poles to S<sub>4</sub>.

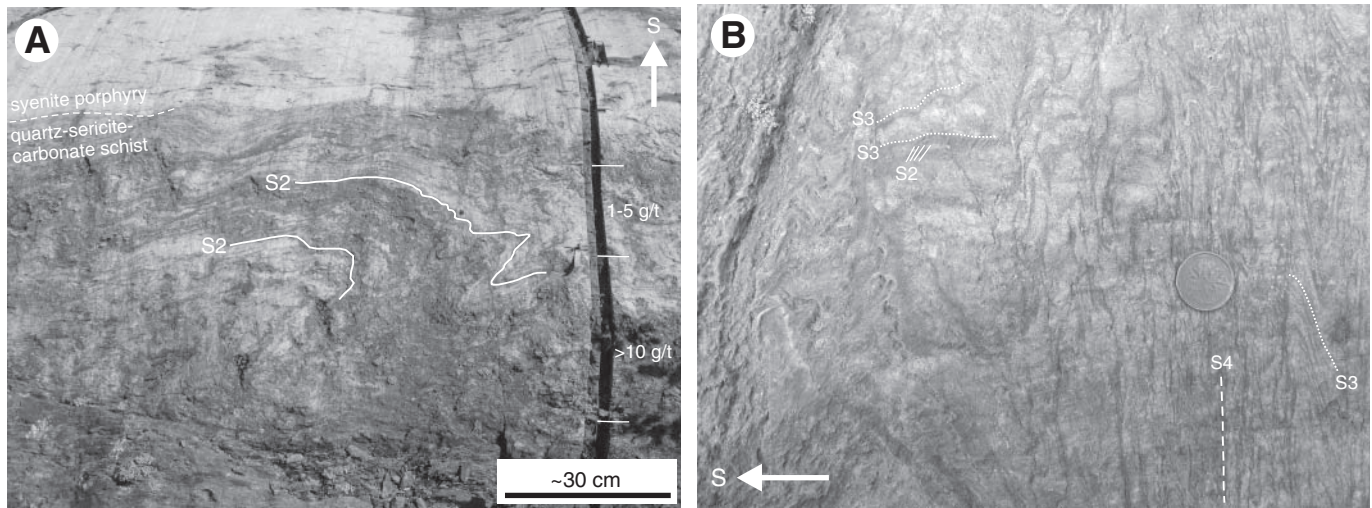


FIG. 16. Overprinting relationships of deformational fabrics in the Upper Canada deformation zone (L stripped outcrop). A. Gold-bearing quartz-sericite-carbonate schists (note gold grade ranges for channel samples), with well-developed  $S_2$  foliation folded about a Z-shaped  $F_4$  fold. B. North-striking  $S_3$  foliation, folded and transposed parallel to  $S_4$ .  $S_2$  is preserved in some  $S_3$  microlithons.

clear association with major steeply dipping faults, these veins are classified as “break ore” following the terminology in use at the Macassa mine.

Veins along the '04 Break strike  $045^\circ$  to  $070^\circ$  and dip  $60^\circ$  to  $80^\circ$  south (near parallel to the host structure) with locally shallower and steeper dips. The veins occupy the main slip surface of the fault but also occur along secondary parallel fractures adjacent to the fault. The veins are typically 15 to 50 cm thick and consist largely of milky white quartz; discontinuous lenses of dark gray quartz (Fig. 18A, B) are relatively rare. Some veins are slightly oblique to the '04 Break and terminate abruptly against the main chlorite-coated slip surface, probably due to postore movements along the fault. Contacts between the veins and wall rocks are sharp, although, less

commonly, the veins are flanked by sheeted veinlet zones. In some cases (e.g., the Discovery outcrop vein), wall rocks are foliated parallel to the veins over a distance of 0.5 to 1 m from vein contacts (Fig. 18C).

The textures of break veins vary along and across strike. Massive sections of veins are filled with relatively uniform white quartz. Banded sections are characterized by irregular bands and lenses of darker quartz, by sharp slip surfaces and stylonitic bands coated with fine molybdenite and graphite, and by 0.5- to 5-cm-thick slivers of typically nonfoliated wall rocks, which are oriented parallel to the vein walls (Fig. 18B) and were probably incorporated into the veins through crack-seal incremental vein opening. Relatively rare are 1- to 3-mm-thick contact-parallel discontinuous sericitic streaks and lenses

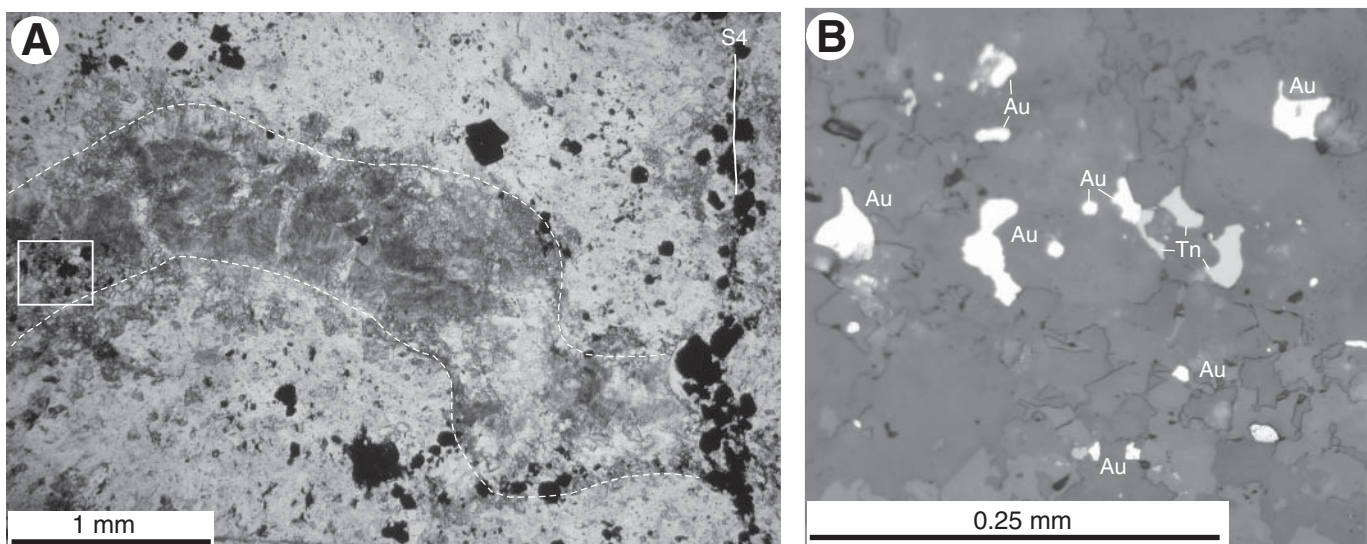


FIG. 17. A. Photomicrograph (transmitted plane-polarized light) of a buckled ( $F_4$ ) gold-bearing quartz-carbonate veinlet transected by an  $S_4$  cleavage plane. B. Higher magnification view of rectangular area in (A). Gold and tennantite hosted by carbonate-rich aggregate. Reflected plane-polarized light.

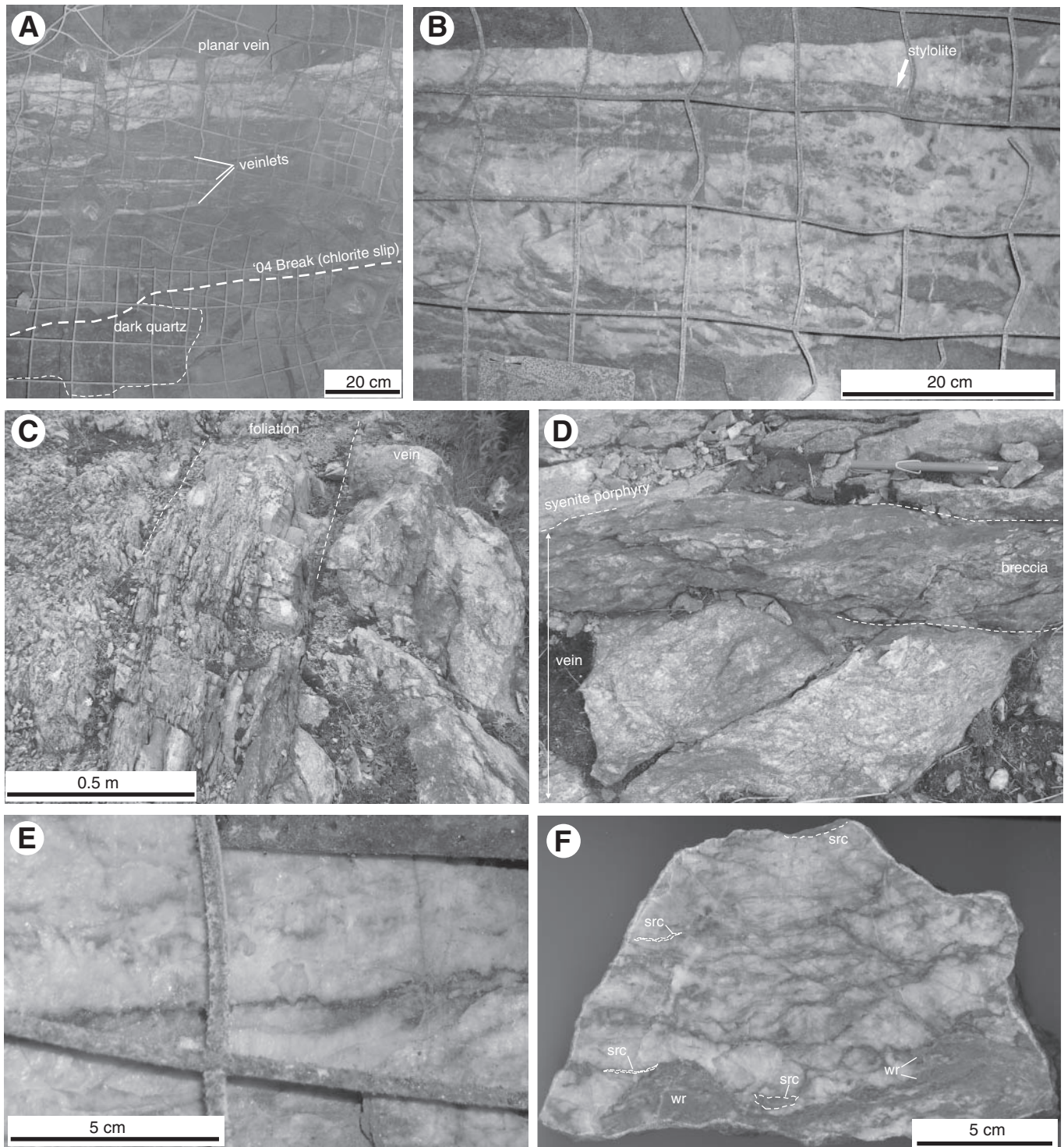


FIG. 18. A. Gold-bearing veins associated with the '04 Break (slope 4940, Macassa mine), showing a planar white quartz vein, small break-parallel quartz veinlets, and a lens of dark gray quartz. Back and north wall of drift, looking north-north-west. B. Vein along the '04 Break, Macassa mine. Note sharp vein contacts, stylolitic surface, slabs, and angular fragments of unfoliated host rock. C. Foliation in the host syenite porphyry along the north contact of the Main Break vein (Discovery outcrop). Looking east. D. Band of breccia consisting of quartz fragments in dark gray cement along the north contact of the Main Break vein at Discovery outcrop. Plan view, looking north. E. Close-up view of a stylolitic band, within a '04 Break vein, Macassa mine. F. Polished slab of the Main Break vein, Lake Shore mine, east of shaft 5. The vein contains thin sericitic lenses (src) and inclusions of strongly sericitized wall rocks (wr).

enclosed in quartz (Fig. 18F). The molybdenite-graphite-coated stylolites, which probably represent modified slip surfaces, locally contain gold and telluride minerals, as well as pyrite and chalcopyrite. They are parallel to the vein boundaries and are marked by 2- to 15-mm-long ragged teeth oriented roughly northwest-southeast (Fig. 18E). Another, very typical vein texture is defined by the presence of angular unrotated wall-rock fragments (0.5–10 cm diam) cemented by white quartz (Fig. 18B). Some of the fragments are coated by dark quartz or molybdenite-graphite rims that are 0.5 to 2 mm thick.

The gold-bearing quartz, which acts as cement between wall-rock fragments, is brecciated in some of the break veins. For example, large parts of the Teck Hughes 1 vein consist of breccia, in which angular (0.5–3 cm) white quartz clasts are surrounded by a dark gray matrix of fine-grained (0.01–0.02 mm) sericite and subordinate quartz, with abundant finely dispersed nonreflective opaque matter, possibly graphite and/or molybdenite (Fig. 19). Gold and tellurides (0.01–0.02 mm) are present both in the quartz fragments (Fig. 19B) and (mostly) in the dark sericite-rich matrix. Some telluride grains fill interstices between variably oriented sericite flakes (Fig. 19C–E), indicating that they crystallized simultaneously with or shortly after sericite, and, consequently, that brecciation and formation of the sericitic matrix overlapped with mineralization. A discontinuous, ~5-cm-wide, band of similar breccia occurs along the north contact of the Discovery outcrop vein (Fig. 18D).

Hanging-wall veins vary in orientations from shallowly ( $10^{\circ}$ – $50^{\circ}$ ) to steeply ( $60^{\circ}$ – $70^{\circ}$ ) south dipping and in thickness from 5 to 100 cm. A few veins dip steeply ( $60^{\circ}$ – $70^{\circ}$ ) to the north. Shallowly dipping veins hosted by bedded tuffs tend to be parallel to bedding; veins near intrusive contacts are roughly parallel to contact surfaces. Virtually all examined hanging-wall veins (including the shallowly dipping ones) are spatially associated with minor faults or shear fractures (Fig. 20). The textures and mineralogy of hanging-wall veins are overall similar to those of the break veins.

The presence of white and gray to dark gray quartz is typical for all vein types. In thin section, white quartz, which makes up the bulk of vein fillings, is medium to coarse crystalline, largely anhedral or, less commonly, subhedral to euhedral. The most common grain size is 1 to 3 mm; some euhedral to subhedral prismatic crystals are up to 20 mm long. Large euhedral-subhedral prismatic crystals are oriented either randomly or at high angles to the vein walls (Fig. 21A, B). In some veins, wall-rock fragments are overgrown by radiating prismatic quartz crystals.

The darker (gray to almost black) vein filling consists of finer (0.01–0.1 mm) quartz (Fig. 21A, B) commonly accompanied by variable amounts of sericite, carbonate, and feldspar. The dark coloration is largely due to the presence of small opaque particles (0.01–0.05 mm), which are non-reflective in polished thin sections (Fig. 21C, D). These opaque particles could be molybdenite or graphite flakes that are too small and insufficiently polished to be reflective or, alternatively, they could consist of a noncrystalline carbonaceous substance. Very fine grained gold, tellurides, and pyrite are present in the dark quartz of some of the veins (Fig. 21C, D).

Dark, finer-grained quartz commonly fills interstices between or entirely encloses coarser white prismatic quartz crystals (Fig. 21A, B). In some veins dark quartz is present in multiple, roughly concordant bands or lenses, and variations in the abundance of wall-rock fragments and of dark and white vein fillings define the banded texture of the veins. Dark, fine-grained quartz may also fill irregular thin fractures in white quartz. Relatively rarely, fine-grained dark gray quartz occurs without white quartz, as lenses along the '04 Break (e.g., Fig. 18A)

*Postore veins:* Barren, postore veins occur along ore-hosting and late postmineralization faults; they either cut across or are parallel to the auriferous veins. The veins consist of translucent quartz, pink or white carbonate, dark green chlorite occurring as rosettes (3–5 mm) and thin bands, and minor

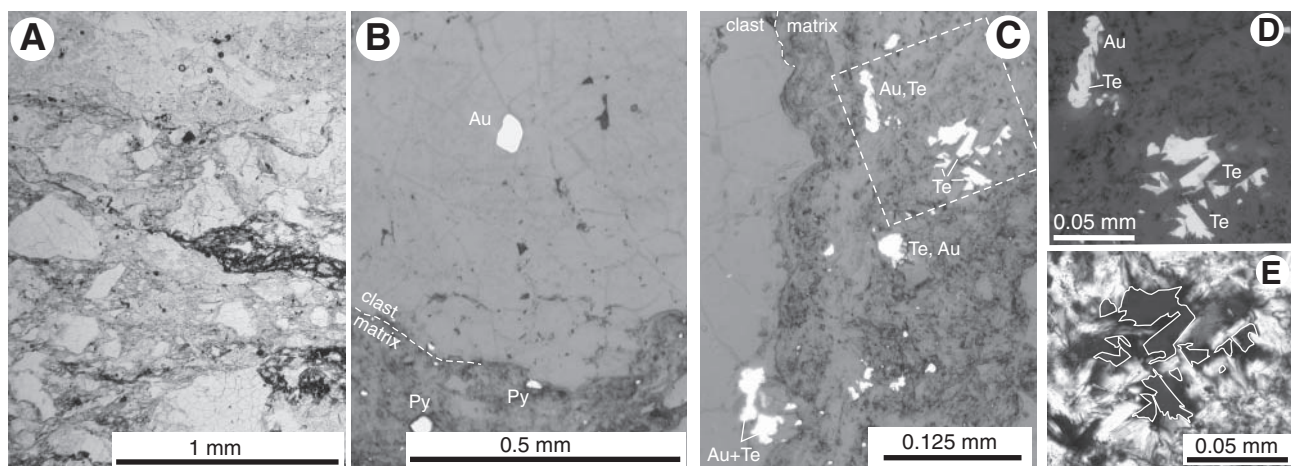


FIG. 19. Photomicrographs of breccia from the Teck-Hughes 1 vein. A. Angular quartz fragments within a sericitic matrix with subordinate fine-grained quartz and fine opaque particles, transmitted plane-polarized light. B. Gold grain in a quartz fragment, reflected plane-polarized light. C. Tellurides (Te), gold (Au), and pyrite (Py) in sericitic matrix; the shape of telluride grains is due to crystallization in interstices of sericite flakes (reflected plane-polarized light). D. Close-up view of rectangular area in (C), reflected plane-polarized light. E. Magnified view of the right-hand bottom part of (D), transmitted cross-polarized light. Tellurides fill interstices between variably oriented sericite flakes.

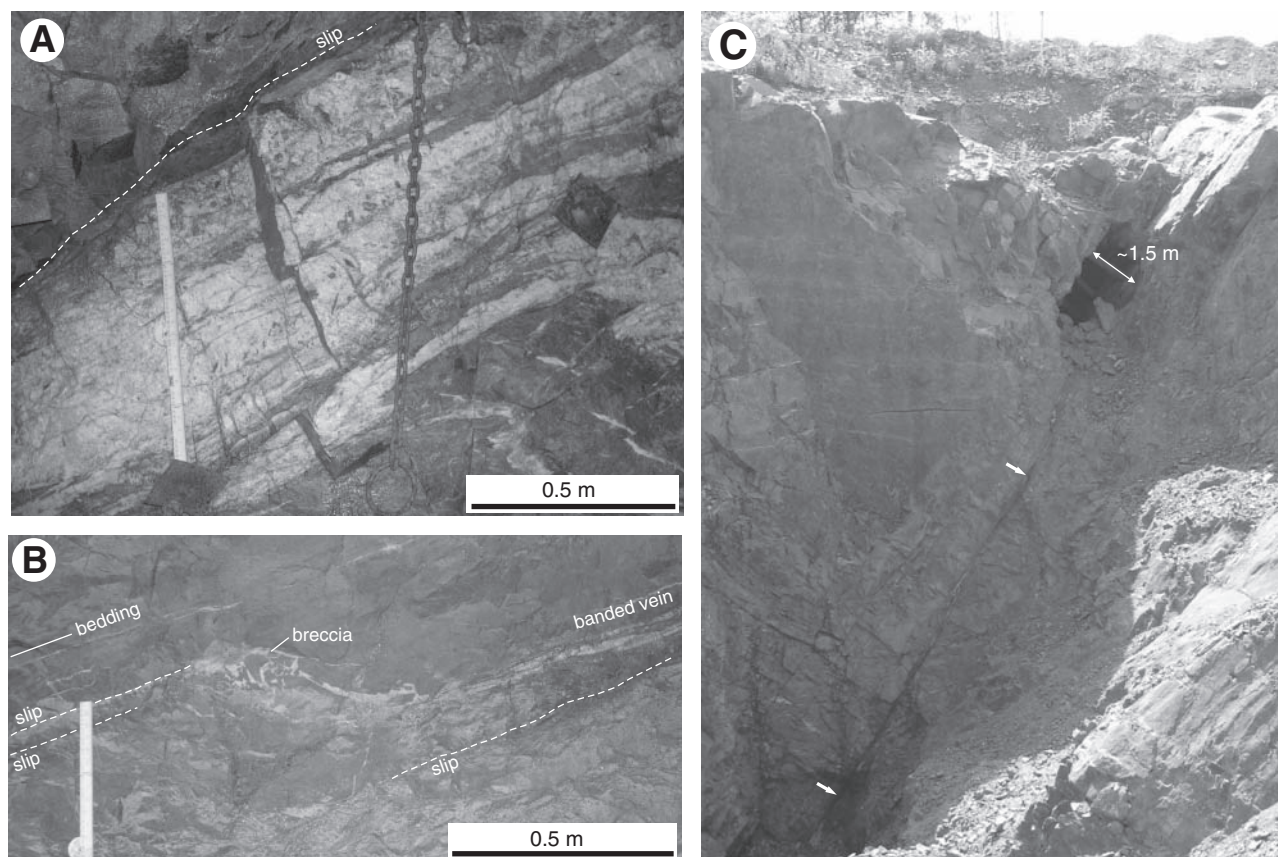


FIG. 20. Examples of shallow- to moderate-dipping hanging-wall veins. A. Vein hosted by mafic syenite and spatially associated with a slip surface (stope 4206-S3, Macassa mine). B. Bedding-parallel vein in tuffs, associated with molybdenite-graphite coated slips. A discordant segment of the vein consists of breccia (wall-rock fragments cemented by quartz). Stope 5030, Macassa mine. C. Remote view of the "E" vein in the proximal hanging wall of the Main Break (Teck-Hughes property, looking west). The vein is hosted by a discrete fault (white arrows).

pyrite and chalcopyrite. Postore barite and selenite veinlets are also common.

**Hydrothermal alteration:** Gold-bearing quartz veins at Macassa are accompanied by typically weak to moderate carbonatization and minor sericitization and silicification of immediate host rocks. Altered rocks along the vein contacts, as well as rock fragments within the veins, invariably contain disseminated pyrite. The syenitic rocks and tuffs along the ore-hosting faults and veins have a red hue due to very fine, dispersed inclusions of hematite, especially in K-feldspar, although how, and if, this hematitization relates to gold mineralization is unclear. Strong carbonate alteration of the cataclases along the Main Break and '04 Break is equally present in mineralized and unmineralized fault segments. It is probably unrelated to mineralization and could have occurred either before or after the formation of the gold-bearing veins (Thomson et al., 1950).

In the central part of the Kirkland Lake deposit (Lake Shore, Wright-Hargreaves, and Teck-Hughes mines), auriferous veins are commonly accompanied by relatively strong sericitization. New observations agree with previous descriptions (Thomson et al., 1950), suggesting that sericitic alteration is closely related to gold mineralization. In the veins, gold and tellurides are commonly associated with sericite, for example, localizing in sericite streaks enclosed by vein quartz

or occurring in the sericite-rich matrix of brecciated veins (Fig. 19C-E). Thin quartz veinlets in the mineralized zone of the Mud Break are surrounded by well-defined sericite alteration halos (Fig 8F).

Chloritization along fault slips, characteristic of the Macassa mine, probably postdates gold mineralization. Gold-bearing veins are spatially associated with chlorite-coated slip surfaces, but chloritization is controlled by fault and fracture slips rather than by the auriferous veins, because it also occurs (without notable decrease in intensity) along barren fault intervals. Chlorite is not a major component of mineralized veins. Apart from slickenlined vein walls coated by chlorite, there is no pronounced bulk wall-rock chloritization along contacts of auriferous veins. Angular rock fragments enclosed in veins also are not chloritized. There are no chlorite gouge clasts or chloritic slip bands among contact-parallel wall-rock slivers incorporated into auriferous veins. Where chlorite is present in veins, it texturally postdates mineralized quartz; that is, it coats fractures or occurs in selvages of crosscutting late barren quartz-carbonate veinlets. On the other hand, dark green chlorite is commonly present as films in selvages and, in places, as rosettes in late, barren, quartz-carbonate veins and veinlets. Thus chloritization along major fault planes is probably associated with late, postmineralization hydrothermal activity.

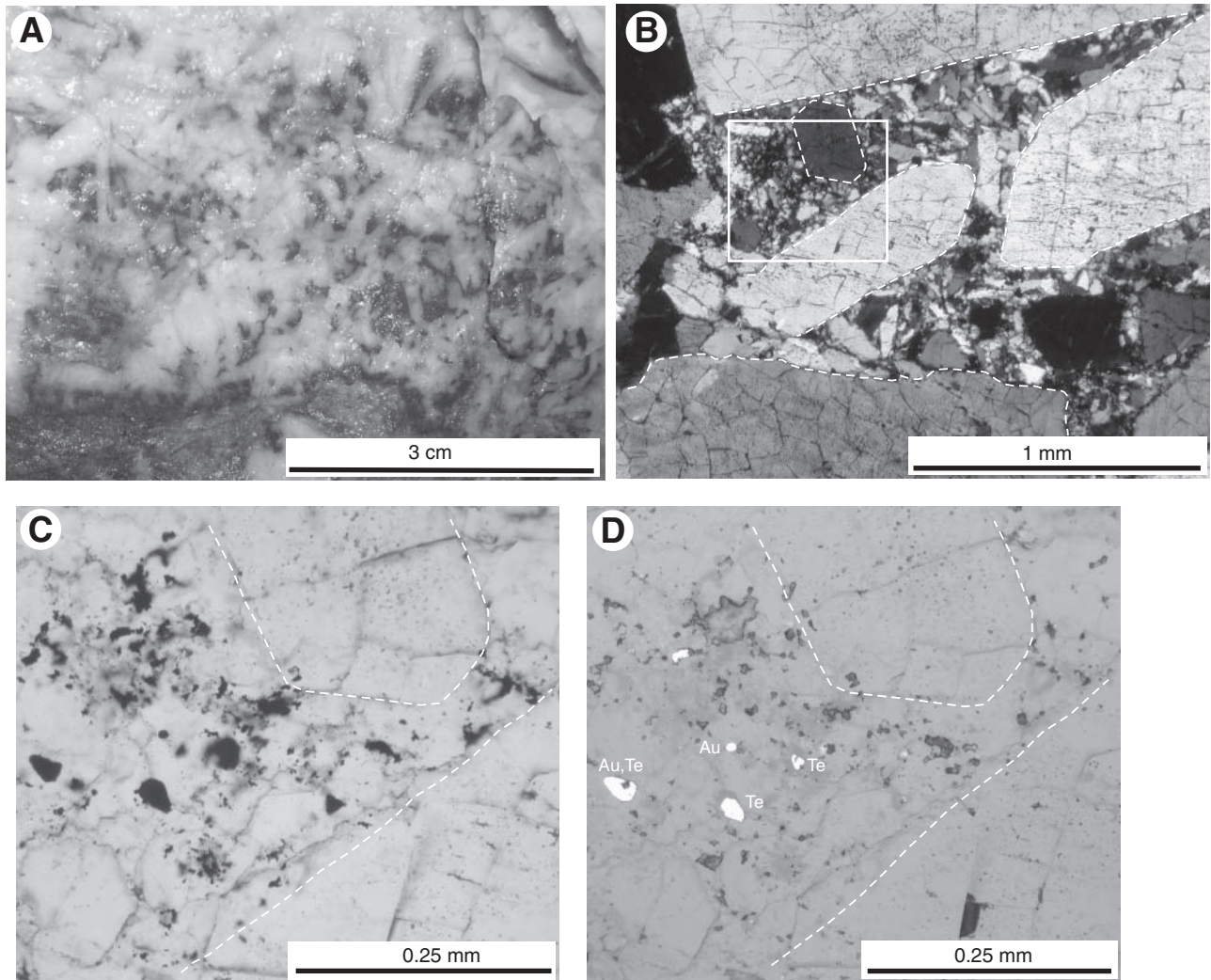


FIG. 21. A. Dark gray, fine-grained quartz filling interstices between randomly oriented coarser prismatic white quartz crystals (vein 4206-S3, Macassa mine). B. Transmitted cross-polarized light photomicrograph of the same vein as in (A); fine-grained quartz in interstices between coarser prismatic quartz crystals. C. Higher magnification photomicrograph of the rectangular area in (B), transmitted plane-polarized light. D. Same view as in (C), reflected plane-polarized light. Note presence of gold (Au), altaite telluride (Te), and opaque nonreflective particles in the dark fine-grained quartz.

*Geochemistry of gold-bearing veins:* Geochemical data for auriferous quartz vein samples are listed in Table A2. All samples are characterized by high Te, Mo, Pb, Ag (although for most samples with  $\text{Au} > 50$  g/t,  $\text{Au}/\text{Ag}$  ratios exceed 10), sporadically high Cu, and low As. The most salient feature is the strong positive correlation between tellurium content and gold values (Fig. 22). Previously published analyses of bulk ore samples from Lake Shore and Kirkland Lake Gold mines (Todd, 1928; Thomson et al., 1950) show similar gold-tellurium relationships, indicating that the geochemical data presented here is representative of Kirkland Lake mineralization in general (Fig. 22). This strong correlation suggests that gold and tellurides likely precipitated simultaneously through the same depositional mechanisms. Although the mineralized veins have high molybdenum concentrations, there is no statistically significant correlation between molybdenum and gold contents.

*Intramineral dikes:* The intramineral dikes are observed in underground workings at the Macassa mine (Still, 2001) and on surface outcrops. They are 2 to 5 cm to 1.5 m thick, light gray to grayish green on fresh surface, and light to dark brown on weathered outcrop surface. They generally have steep dips ( $65^\circ$ – $90^\circ$ ) and northeast strikes, although some dikes exhibit abrupt changes in orientation. The dikes have sharp, although commonly irregular, intrusive contacts that are locally marked by splintery microapophyses penetrating into the host rocks. Angular wall-rock xenoliths are common within the dikes. Immediate endocontacts of some dikes are marked by thin (1–3 mm) light-colored rims, interpreted as chilled margins.

Macroscopically, the dikes are largely aphanitic, with barely visible small (<1 mm) dull-green altered mica flakes. Sparse coarser biotite (1–3 mm) and light-green euhedral prismatic pseudomorphs (1–3 mm) are present in some dikes. In thin section, the rocks contain 10 to 20 vol percent variably altered

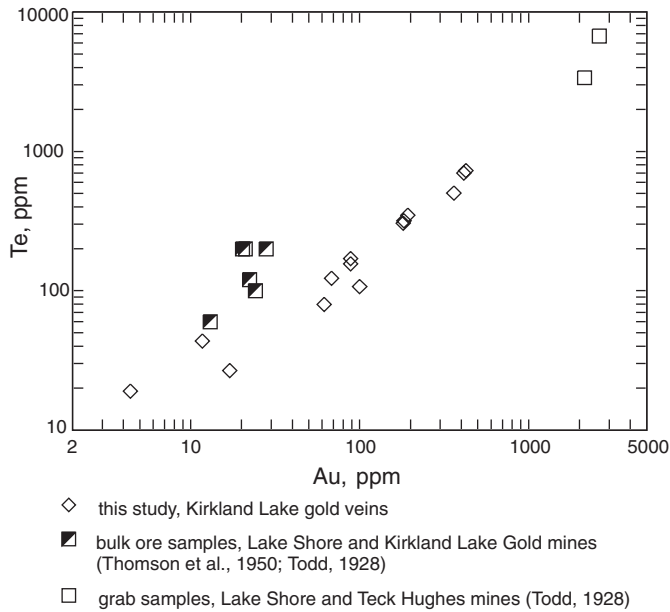


FIG. 22. Au-Te plot for representative samples of Kirkland Lake gold veins (data from Table A2, Ispolatov et al., 2005, and published historical data of Todd, 1928, and Thomson et al., 1950). Samples from Kirkland Lake gold veins of this study and grab samples of Todd (1928) show well-defined correlation between Au and Te and Au/Te <1. Bulk-ore samples show similar relationships; a slight deviation from the trend is probably due to a low sensitivity of Te analyses of these samples (for most bulk samples, Te is reported in wt %, to the second decimal).

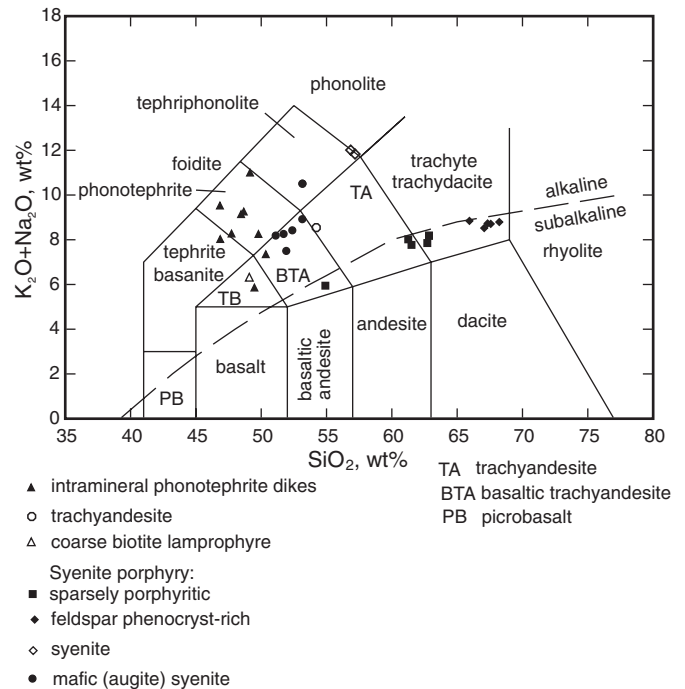


FIG. 23. Silica-total alkali plot (Irvine and Baragar, 1971; Le Bas et al., 1986) for intrusive rocks of the Kirkland Lake gold deposit (geochemical data are from Table A5 and Ispolatov et al., 2005).

thin biotite flakes (0.25–0.5 mm) and relatively sparse rounded or ovoid grains (0.25–0.4 mm) completely replaced by fine-grained feldspar. The prismatic pseudomorphs present in some dikes consist of carbonate, chlorite, sericite, ±epidote, and acicular amphibole and probably represent altered mafic (pyroxene?) phenocrysts. Coarser (1–3 mm) biotite grains show signs of resorption and are likely xenocrystic. The matrix of the dikes is aphanitic and variably altered to sericite, chlorite, and carbonate.

Although total alkali contents and K<sub>2</sub>O/Na<sub>2</sub>O ratios of the dikes vary broadly, probably due to alteration, most dikes plot as phonotephrite on a total alkali versus silica diagram (Fig. 23). Binary plots of relatively immobile elements (e.g., Zr-TiO<sub>2</sub> and P<sub>2</sub>O<sub>5</sub>-V, Fig. 24) confirm that dikes from underground workings and surface outcrops belong to one coherent group that is geochemically distinct from other alkalic intrusive rocks. Primitive mantle-normalized spider plots of the phonotephrite dikes show the same strongly fractionated REE and pronounced Nb, Ti, and Sc lows (Fig. 25), which are typical of Timiskaming volcanic rocks and related syenitic plutons (e.g., Ben Othman et al., 1990; Rowins et al., 1993). Thus, the dikes, although younger, probably represent the same magmatic cycle as stratified Timiskaming volcanic rocks and alkalic intrusions.

Relationships between the phonotephrite dikes and mineralization are observed underground at Macassa. The dikes are generally parallel to the veins, suggesting that they were emplaced in the same system of fractures as the mineralized veins. Most dikes bordering mineralized veins are variably altered (carbonate, sericite, ±quartz), contain disseminated

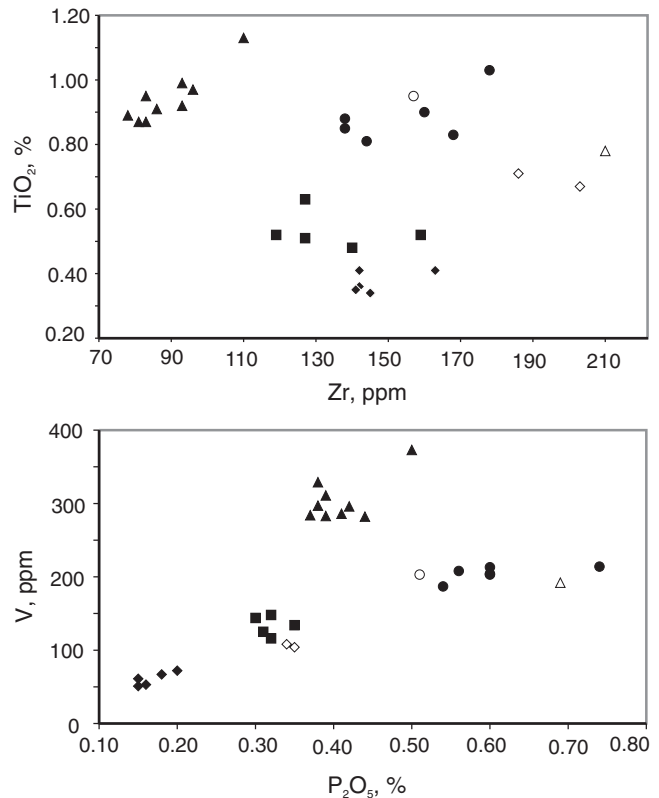


FIG. 24. Zr-TiO<sub>2</sub> and P<sub>2</sub>O<sub>5</sub>-V binary plots for intrusive rocks of the Kirkland Lake gold deposit (symbols are the same as in Fig. 23, geochemical data are from Table A5 and Ispolatov et al., 2005). Plots are intended to illustrate differences between trace element signatures of intrusive rocks, without applying to magma source or tectonic setting.

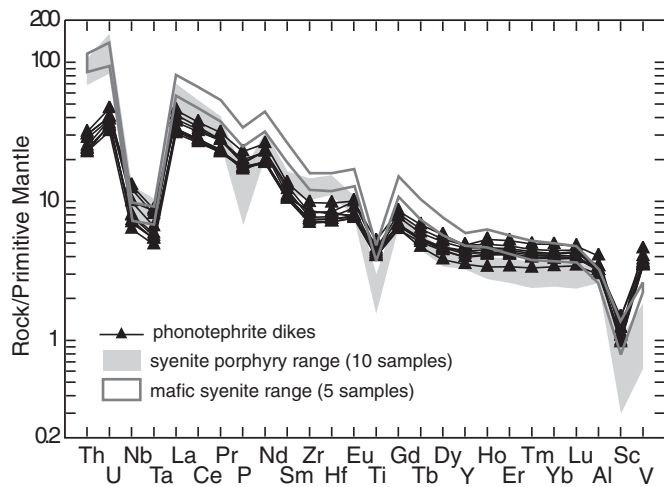


FIG. 25. Primitive mantle-normalized plot for intramineral phonotephrite dikes, mafic syenites, and syenite porphyries. Data ranges for mafic syenites, and syenite porphyries are based on five and 10 samples, respectively. Data are from Table A5 and Ispolatov et al. (2005); normalizing factors are from Sun and McDonough (1989).

pyrite, and show elevated gold contents. However, at one location (slope 4528 MCF), a 20- to 70-cm-thick dike in direct contact with a gold-bearing quartz vein contains fragments of the quartz veins (0.3–1 cm) entirely enclosed in the dike matrix (Fig. 26). The dike contact is irregular and is marked by splintery, millimeter-thick microapophyses that extend from the dike into the gold-bearing quartz vein. The dike is only weakly altered, whereas the host mafic syenite along the vein contact and mafic syenite fragments within the vein are strongly altered and contain abundant pyrite. These relationships, along with hydrothermal alteration and elevated gold values in other dikes, indicate that the dikes were emplaced during the period of mineralization.

The relative structural timing of the intramineral dikes is difficult to determine because in underground workings of

Macassa mine, dikes, host syenitic rocks, and tuffs are generally unfoliated. Although a few dikes show a weak foliation along their contacts, this foliation probably reflects local contact-parallel slip and cannot be positively correlated to regional fabrics. On surface, five of six dikes observed in outcrops are moderately to strongly foliated by  $S_4$ . On an outcrop about 850 m north of the Main Break (Fig. 27), a syenite porphyry sill and Timiskaming tuff are folded about a southwest-plunging  $F_4$  synform and overprinted by northeast-striking  $S_4$  (Fig. 27B,C). The contact is transected by two phonotephrite dikes that show no differences in grain size, phenocryst content and composition, or other primary magmatic textures. The larger 1- to 1.5-m-thick dike is parallel to  $S_4$ ; it shows (both in outcrop and thin section) a strong penetrative  $S_4$  foliation and offsets (with apparent dextral sense) the tuff-syenite porphyry contact by 1 to 1.5 m. The smaller (3–5 cm) dike is also parallel to  $S_4$ , except at the tuff-syenite contact where it follows the southeast-trending contact over 20 cm. This small dike lacks penetrative  $S_4$  foliation. The deformation is manifested by rare contact-parallel irregular pressure-solution cleavage planes, which are visible only in thin section and may represent a very weak  $S_4$ . A penetrative  $S_4$  foliation is not seen even where the dike is parallel to the tuff-syenite contact and thus favorably oriented to develop a strong cleavage by layer-parallel homogeneous shortening. These relationships between the dikes,  $F_4$ , and  $S_4$  suggest that the emplacement of the dikes overlapped with  $D_4$  and the larger dike was emplaced earlier than the smaller one.

#### U-Pb and Re-Os Geochronology

Selected samples from the Gauthier and Teck mapping areas were dated by U-Pb and Re-Os methods. Dating by U-Pb methods included isotope dilution-thermal ionization mass spectrometry (ID-TIMS), and in situ sensitive high-resolution ion microprobe (SHRIMP) analyses that were done, respectively, at the Jack Satterly Geochronological Laboratory at University of Toronto and at the Geological Survey of Canada in Ottawa. Re-Os analyses were carried out at the

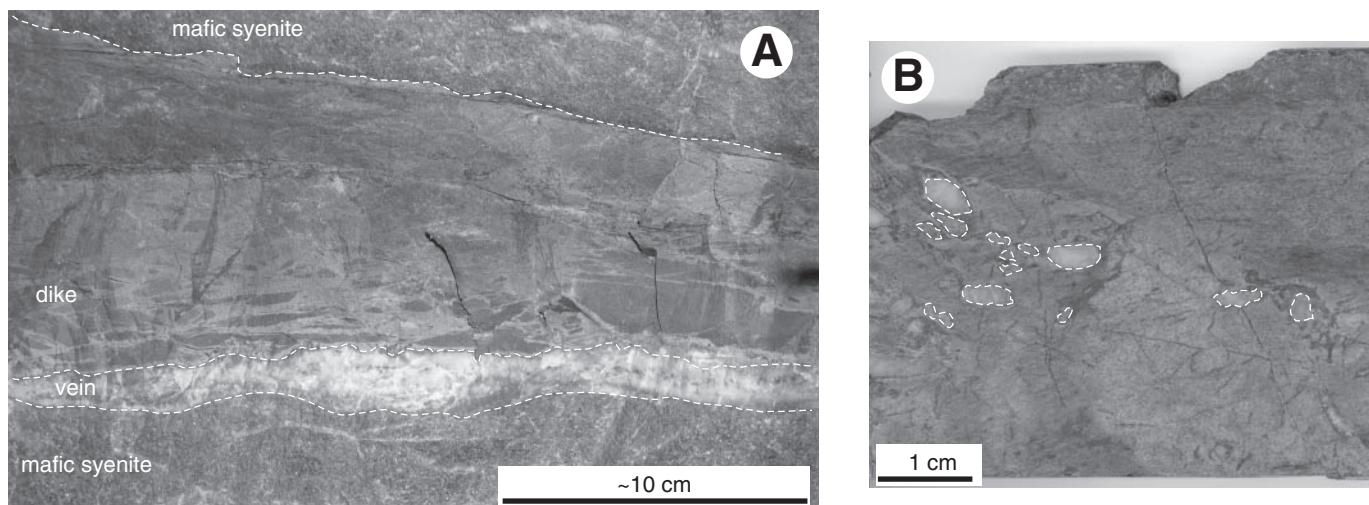


FIG. 26. Intramineral phonotephrite dike, slope 4528 MCF, Macassa mine. A. Intramineral dike parallel to the gold-bearing vein exposed in the back of the slope. B. Fragments of vein quartz (highlighted) entirely enclosed within the dike matrix (a cut slab).

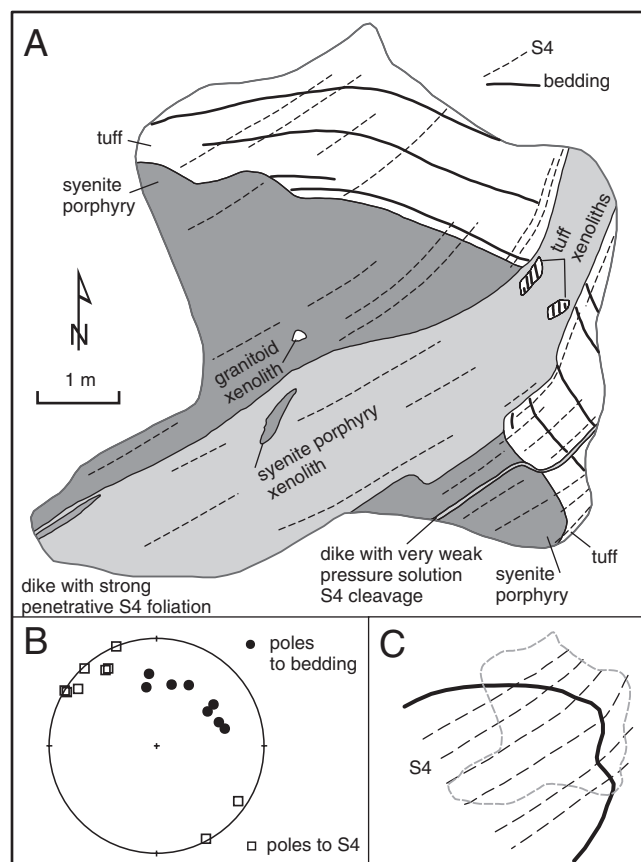


FIG. 27. A. Outcrop sketch (UTM zone 17, NAD83 568570mE/5333145 mN), showing approximately concordant contact of tuff and syenite porphyry crosscut by two phonotephrite dikes. The thick dike is strongly foliated by  $S_4$ , whereas the thin dike is very weakly foliated. B. Equal-area lower hemisphere projection of structural data from the outcrop. C. Schematic view of the southwest-plunging  $F_4$  synform exposed on the outcrop.

Radiogenic Isotope Facility at the University of Alberta. Detailed analytical procedures for the U-Pb and Re-Os methods are provided in Ayer et al. (2005) and Selby and Creaser (2004). Isotope analytical results are listed in Tables A1, A3, and A4 and are summarized below. Analytical uncertainties for ID-TIMS and SHRIMP data are reported at 2 and 1 $\sigma$ , respectively, and Re-Os uncertainties are quoted at 2 $\sigma$ .

#### Supracrustal sedimentary and volcanic rocks (Gauthier mapping area)

Two samples of supracrustal rocks from the Gauthier mapping area were dated by the U-Pb ID-TIMS method. Sandstone sample 03VOI0570-1 is from the thick turbiditic unit north of the Larder Lake-Cadillac deformation zone (unit 2, Fig. 2). The age and stratigraphic setting of this unit are not well constrained. Hyde (1980) included these turbidites within the Timiskaming assemblage, as lateral equivalents to the more typical Timiskaming alluvial-fluvial clastic rocks and alkalic volcanics. Corfu et al. (1991) and Mueller et al. (1994) interpreted the turbidites as older, pre-Timiskaming rocks. Corfu et al. (1991) also proposed that Timiskaming alluvial-fluvial sedimentation and volcanism took place primarily during 2680 to 2677 Ma. This time interval is constrained by

maximum depositional ages of fluvial sandstones north of Kirkland Lake and south of Larder Lake ( $\leq 2680 \pm 3$  and  $\leq 2679 \pm 3$  Ma, detrital zircon U-Pb ages) and by the age of a volcanic agglomerate north of Larder Lake ( $2677 \pm 2$  Ma, zircon U-Pb; Corfu et al., 1991). Therefore, if the turbidites were deposited prior to fluvial Timiskaming sedimentation, they would likely be older than ca. 2680 Ma.

Sample 03VOI0570-1 yielded six single-grain detrital zircon ages clustering mainly between  $2677.7 \pm 3.1$  and  $2682.4 \pm 2.0$  Ma, whereas one grain is considerably older  $2769.8 \pm 1.7$  Ma (Table A1, Fig. A1-A). The youngest age of  $2677.7 \pm 3.1$  Ma constrains a maximum depositional age for this turbiditic sandstone. It overlaps with the ca. 2679 to 2680 Ma maximum depositional ages of alluvial-fluvial Timiskaming sandstones and with the  $2677 \pm 2$  Ma age of Timiskaming volcanic agglomerate (Corfu et al., 1991). These age relationships confirm that turbidites north of Larder Lake-Cadillac deformation zone belong to the Timiskaming assemblage.

The second sample (03VOI0422-1) was collected from a Timiskaming volcanic flow 650 m southeast of the former Upper Canada shaft 1. Zircon fractions comprising single or small multiple grains are concordant or nearly concordant and yield  $^{207}\text{Pb}/^{206}\text{Pb}$  ages ranging from 2668.3 to 2670.1 Ma (Table A1, Fig. A1-B). The strongly colinear nature of the data permits a regression fit through the origin and provides an upper intercept age of  $2669.6 \pm 1.4$  Ma (71% probability of fit, MSWD = 0.34; Fig. A1-B). Two other fractions yield distinctly older ages, 2694 and 2676 Ma, presumably due to inheritance from older sources. The  $2669.6 \pm 1.4$  Ma age is interpreted as the best estimate of the crystallization age of the flow. This age is younger than any previously published Timiskaming detrital zircon ages in the Kirkland Lake-Larder Lake area. However, it correlates well with the maximum depositional age of sandstones and conglomerates in the uppermost Three Nations Formation in the Timiskaming assemblage north of Timmins (2669–2670 Ma; Ayer et al., 2003). In summary, the new U-Pb data presented here along with the previously published results by Corfu et al. (1991) imply that Timiskaming sedimentation and volcanism in the Larder Lake area initiated at ca. 2677 and continued to ca. 2670 Ma.

#### Kirkland Lake gold deposit

One syenite porphyry and four mineralized veins were analyzed using the U-Pb and Re-Os methods to provide constraints on the ages of hydrothermal activity, deformation, and magmatism in Kirkland Lake. Two intramineral dikes were also sampled but did not yield minerals amenable to precise U-Pb dating. The syenite porphyry sample (03JAA0006) is from the Discovery outcrop of the Main Break on the former Wright-Hargreaves property. Three of the four molybdenite-bearing mineralized vein samples are from stopes 4744, 4247-3, and 5030 of the Macassa mine; the fourth sample, from the presently inaccessible 5400-ft level of Macassa mine (Tegren-Gracie claim), comes from the collection of the Ontario Geological Survey Resident Geologist office in Kirkland Lake.

U-Pb dating of zircons from the syenite porphyry returned complex results. The sample yielded a zircon population consisting largely of colorless to pale brown subhedral prisms, slightly flat to square in cross section, and variably cracked and clouded with inclusions. The largest, clear and crack-free

grains are colorless or pale brown irregular crystal fragments, rarely with prismatic crystal faces. Higher quality representative zircons from each morphological group were selected for U-Pb dating and subjected to strong air abrasion treatment prior to analysis. ID-TIMS ages of five single-grain fractions vary from 2700 to 2690 Ma ( $2700.2 \pm 2.9$ ,  $2700.6 \pm 4.4$ ,  $2694.4 \pm 7.4$ ,  $2689.6 \pm 4.7$ , and  $2689.7 \pm 41.3$  Ma; Fig. A1). The youngest single-grain fraction is ca. 2690 Ma, which itself indicates zircon inheritance, since Timiskaming clastic rocks that host syenite intrusions at the Kirkland Lake deposit are younger than 2680 Ma (Corfu et al., 1991). Scanning electron microscope (SEM) imaging shows that most zircons from the syenite porphyry preserve broad internal zoning or have large, locally rounded cores enveloped by very thin, high U, oscillatory-zoned shells or overgrowths (Fig. 28). Although comparatively imprecise relative to individual ID-TIMS analyses, SHRIMP spot ages from zircon cores range from about 2723 to 2675 Ma and are dominated by ca. 2700 Ma ages (Figs. 28, A1). The data are very similar to the ID-TIMS results and essentially confirm the dominantly xenocrystic nature of the zircons in this syenite porphyry intrusion. A single analysis of the center of a heavily cracked grain yielded an age of  $2674 \pm 6$  Ma, but this age likely reflects some secondary Pb loss and is not, in isolation, considered reliable. Few grains

have overgrowths sufficiently thick for analysis. Rare analyzed overgrowths have ages near 2685 Ma (Fig. 28). These ages are still too old to represent the timing of crystallization of the syenite porphyry. We therefore conclude that the zircons might have been inherited from a regional ca. 2685 to 2692 Ma porphyry suite observed throughout the southern Abitibi subprovince. More rigorous interpretation of the results is clouded by the relatively large intrinsic imprecision of the SHRIMP spot analytical data. Two SHRIMP spot ages (one from a diffuse, embayed, unzoned rim) are very young (ca. 2642–2649 Ma) and may be related to a late hydrothermal or metamorphic event manifested in other parts of the Abitibi greenstone belt (Corfu et al., 1989; Jemeliet al., 1990; Bleeker et al., 1999), but the nature of this event and its relationships to gold mineralization remains unknown.

Re-Os results are summarized in Table A4. Four analyzed samples consisted of auriferous quartz veins, with very fine grained molybdenite occurring largely as coatings on slip surfaces and fractures. Due to the very fine grain size of molybdenite, obtained mineral separates were not completely pure. XRD scans of the separates, although generally complicated by interference from pyrite and silicate impurities, indicate predominance of the 2H molybdenite polytype. Analyses of two aliquots derived from two separate rock fragments of

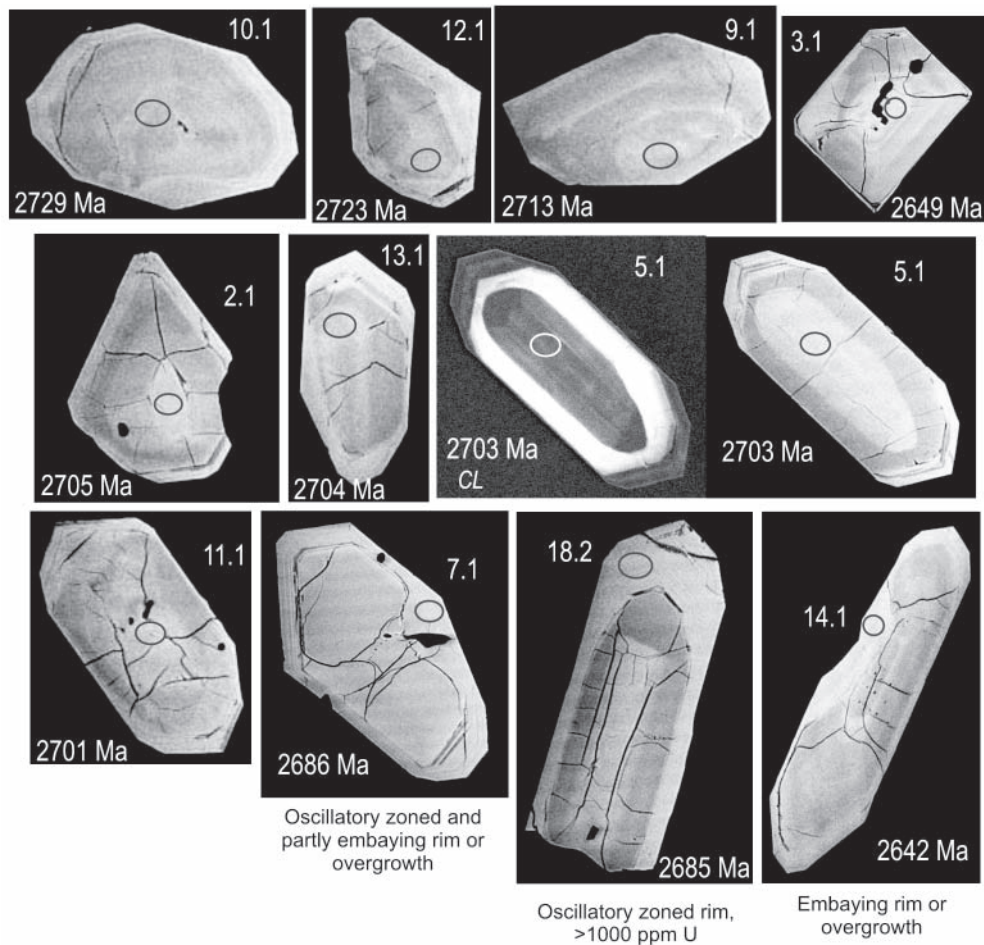


FIG. 28. Backscattered electron and cathodoluminescence images of zircon from syenite porphyry sample 03JAA0006. Spot locations, numbers, and ages correspond to SHRIMP analyses listed in Table A3.

sample 4247-3 returned conflicting Re-Os model ages of  $2773 \pm 7$  and  $2710 \pm 7$  Ma. Sample 5030, represented by three fractions of molybdenite concentrate drilled from a single fracture surface, yielded partially inconsistent ages of  $2976 \pm 8$ ,  $2927 \pm 8$ , and  $2977 \pm 8$  Ma. Two splits of concentrate drilled from a single surface on sample Tegen-Gracie produced internally consistent dates of  $2696 \pm 7$  and  $2694 \pm 7$  Ma. Two fractions of a single-spot, drilled aliquot from sample 4744 yielded internally consistent ages of  $2677 \pm 8$  and  $2666 \pm 8$  Ma. This sample was further examined by preparing a full mineral separate from a large rock fragment following Selby and Creaser (2004). Ages of two fractions of this bulk separate,  $2679 \pm 8$  and  $2678 \pm 7$ , agree with each other and with the ages of the drilled concentrate. The four analyses of sample 4744 yield a weighted average Re-Os age of  $2675 \pm 6$  Ma (95% confidence including 0.31%  $^{187}\text{Re}$  decay constant uncertainty, MSWD = 1.2).

The analyzed samples represent a single hydrothermal system and are thus expected to have the same geologic age, within the resolution of the Re-Os method for the Archean. No mineralogical or chemical variations have been noticed between the samples; they all consist of fine-grained molybdenite with similarly low Re content (0.5–0.9 ppm, Table A4; cf. Selby and Creaser, 2004). However, Re-Os model ages range from  $2977 \pm 8$  to  $2666 \pm 8$  Ma, and only ages of sample 4744 (weighted mean  $2675 \pm 6$  Ma) conform with available geologic constraints on the timing of mineralization (i.e., are younger than the maximum depositional age of Timiskaming clastic rocks in the Kirkland Lake area). All other results exceed the age of Timiskaming rocks and cannot have geologic significance. In addition to being anomalously old, results of samples 4247-3 and 5030 are not internally reproducible within  $2\sigma$  analytical uncertainties.

Molybdenite is typically a robust and accurate Re-Os geochronometer (e.g., Stein et al., 2001), but there are cases of poor reproducibility of molybdenite ages, most likely due to intracrystalline decoupling of Re and Os (Stein et al., 2001; Selby and Creaser, 2004). Such decoupling is known to occur in coarse (e.g., 0.5–1.5 cm) molybdenite and especially in Re-poor varieties of the mineral (Selby and Creaser, 2004). Concentrating a larger bulk mineral separate and increasing aliquot size can overcome this phenomenon, essentially by small-scale variations in Re and Os contents (Selby and Creaser, 2004).

The poor reproducibility of Re-Os ages indicates inhomogeneities in the Re-Os systematics of Kirkland Lake molybdenite, which is characterized by very low Re contents. However, Re-Os decoupling, as it is presently understood, cannot fully explain the complexity of Kirkland Lake Re-Os data. The analyzed molybdenite is very fine grained, most aliquots were large (>100 mg), and there were no systematic differences between the ages of large and small aliquots. Rather than randomly scattered ages, as would be expected in the case of diffusion-driven Re-Os decoupling, there is a pronounced tendency for anomalously old ages, some of which are internally reproducible (i.e., ages of the Tegen Gracie sample). Four model ages determined for sample 4744, including two results returned by a more representative bulk separate, show good internal consistency. These ages match independent geochronological constraints, and the weighted mean age of  $2675 \pm 6$  Ma may represent a relatively close approximation

to the geologic age of Kirkland Lake mineralization. However, considering the unexplained complexity of the other Re-Os results and the occurrence of an internally consistent but inaccurate date (Tegen Gracie sample), the Re-Os age of sample 4744 cannot be interpreted as conclusive.

## Discussion

### *Gold mineralization along the Larder Lake-Cadillac deformation zone*

The Anoki and McBean deposits are part of a regional-scale hydrothermal system, which produced the world-class Kerr-Addison-Chesterville deposit, the Omega and Cheminis deposits, as well as several other significant gold occurrences (Thomson, 1941; Thomson and Griffis, 1941; Clark and Bonnar, 1987; Smith et al., 1993). The characteristic features of this system are briefly summarized below.

Mineralization is hosted by a first-order structure, the Larder Lake-Cadillac deformation zone, rather than by second- and/or third-order structures. Mineralized zones are commonly associated with gentle bends along the Larder Lake-Cadillac deformation zone. This association is documented at the McBean deposit (Fig. 11). It is also apparent at the Cheminis, Omega, and, possibly, Anoki deposits (Fig. 29). Within the host deformation zone, mineralization tends to form linear shoots (strike length < dip length) that plunge roughly parallel to the regional stretching lineation ( $L_2$ ): i.e.,  $\sim 50^\circ$  east at McBean (this study),  $\sim 70^\circ$  east at Kerr-Addison (Smith et al., 1993, p. 30), near vertical at Cheminis (longitudinal section in Clark and Bonnar, 1987; structural data in Wilkinson, 1993, p. 142).

Gold occurs mainly in mafic and ultramafic volcanic rocks of the Larder Lake Group (Tisdale assemblage) and is distributed between two principal styles of mineralization. The economically most important style is the pyritic replacement of Fe tholeiitic volcanic rocks, where gold occurs largely as submicroscopic particles in pyrite (Thomson, 1941; Smith et al., 1993; Warwick, 1981; Kishida and Kerrich, 1987). This mineralization, called “flow ore,” accounted for approximately 65 percent of the gold at Kerr-Addison-Chesterville (Smith et al., 1993). Similar replacement ore zones have been mined at the Omega mine (Thomson, 1941) and delineated by underground workings and diamond drilling at the Cheminis (Thomson, 1941; Clark and Bonnar, 1987) and Anoki deposits. The second, less economically important, style of gold mineralization consists of quartz stockworks and veins in carbonate-fuchsite-altered ultramafic rocks (“green carbonate ore”), where coarser native gold is present principally in vein quartz. The two mineralization styles coexist within individual deposits and are probably related to the same hydrothermal episode (e.g., Smith et al., 1993). Carbonate is a significant component of both mineralization styles, which indicates that ore was likely generated by  $\text{CO}_2$ -bearing fluids (Kishida and Kerrich, 1987). Sulfidation of the Fe-rich, high Fe/Mg tholeiitic rocks controlled gold deposition in pyritic replacement mineralization (cf. Phillips et al., 1984; Böhlke, 1988; Smith et al., 1993), whereas gold in quartz veins within carbonate-fuchsite-altered ultramafic rocks was probably deposited through fluid immiscibility (Smith et al., 1993). Several ore zones occur in relatively competent lava flow units (e.g.,

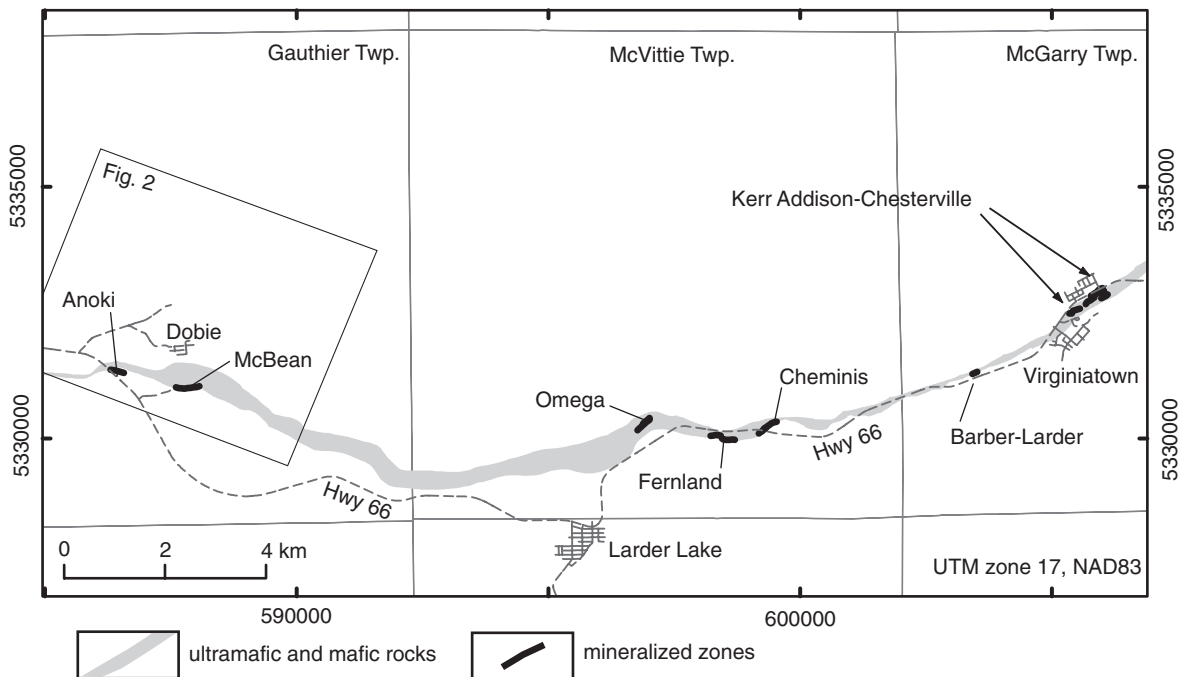


FIG. 29. Location of gold deposits and major occurrences along the Larder Lake-Cadillac deformation zone in the Larder Lake area. Mineralized zones are hosted by a band of intermingled ultramafic and mafic rocks within the Larder Lake-Cadillac deformation zone. The McBean, Cheminis, Omega, and possibly Anoki deposits are spatially associated with bends along the Larder Lake-Cadillac deformation zone. Geology after Thomson (1941) and Smith et al. (1993). Coordinates are UTM zone 17, NAD83.

Omega, Cheminis, Kerr-Addison) that are flanked by rheologically weaker and less permeable talc-chlorite-altered and variably strained ultramafic rocks (e.g., Thomson, 1941; Smith et al., 1993).

The observed localization of syndeformational, "orogenic" gold mineralization in a first-order deformation zone is generally atypical. In most economically significant gold camps associated with regional deformation zones, the largest deposits are hosted by subsidiary, second- or third-order faults and shear zones (Eisenlohr et al., 1989; Robert, 1990; McCuaig and Kerrich, 1998). The unusual localization pattern may be due to the nature of the Larder Lake-Cadillac deformation zone in the Larder Lake area. The lithologic assemblage in the deformation zone includes competent mafic volcanic units intermingled with or enveloped by incompetent and probably impermeable talc-chlorite-altered ultramafic rocks (Thomson, 1941). This association may have been favorable, maintaining isolated discrete permeable fluid conduits within the deformation zone. Rigid tholeiitic volcanic units responded more brittlely, thus enhancing their overall permeability. Rheologically weak talc-chlorite rocks enveloping these permeable zones prevented fluid dispersal and maintained high fluid/rock ratios within fluid pathways. Some of these competent units were also geochemically favorable for sulfidation (i.e., Fe tholeiitic, high Fe/Mg rocks) and thus controlled gold deposition.

#### *Structural timing of gold mineralization along D<sub>2</sub> deformation zones*

The relationships between gold mineralization and deformation are best documented at the Upper Canada mine. S<sub>2</sub>,

the first recognizable deformational fabric in the Upper Canada L zone, is defined by deformed hydrothermal quartz, sericite, carbonate, and pyrite. This suggests that extensive hydrothermal alteration of the rocks occurred before or during D<sub>2</sub>. Gold is sited in S<sub>2</sub>-parallel carbonate-rich veinlets and the best gold grades are in carbonate-rich quartz-sericite-carbonate schists. This similarity in mineral composition of the gold-bearing veinlets and alteration assemblage supports a close interrelationship between veinlet-hosted mineralization and strong carbonatization of the host rocks; that is, both were likely generated by the same CO<sub>2</sub>-bearing fluids. Auriferous quartz-carbonate veinlets record lower D<sub>2</sub> strain than some silica-rich bands in the host rocks, indicating that emplacement of these veinlets and hydrothermal alteration overlapped with D<sub>2</sub> and did not entirely predate it. The plunge of ore zones parallel to the L<sub>2</sub> lineation, and the overprinting of the L zone and individual gold-bearing veinlets by D<sub>4</sub> structures are also consistent with a syn-D<sub>2</sub> timing of mineralization. Based on the summarized evidence, we interpret gold mineralization of the Upper Canada mine as broadly synchronous with D<sub>2</sub>. The presence of sericite, pyrite, ±tourmaline along S<sub>3</sub> and S<sub>4</sub> indicate that hydrothermal activity continued during D<sub>3</sub> and D<sub>4</sub>, however there is no evidence for significant modification (geometrical or compositional) of mineralization.

The Upper Canada gold deposit is likely related to gold mineralization along the Larder Lake-Cadillac deformation zone. The Upper Canada deformation zone is a splay of the Larder Lake-Cadillac deformation zone (D.J. Toogood, unpub. report for Queenston Mining Inc., 1989, 57 p.); both deformation zones are D<sub>2</sub> structures and could have been

hydraulically connected during D<sub>2</sub>. In the same manner as the Upper Canada deposit, gold mineralization along the Larder Lake-Cadillac deformation zone is accompanied by carbonate-rich alteration assemblages, which reflects its origin from similar CO<sub>2</sub>-rich fluids. Mineralized zones at Kerr-Addison-Chesterville, Cheminis, McBean, and Anoki also plunge roughly parallel to the L<sub>2</sub> lineation. S<sub>2</sub> foliation at McBean is defined by alteration minerals and is overprinted by D<sub>4</sub>, as observed at the Upper Canada L zone. These relationships suggest that gold deposits hosted by the Larder Lake-Cadillac deformation zone, similarly to the Upper Canada deposit, formed during D<sub>2</sub> and can be interpreted as belonging to the syndeformational, "orogenic" type.

#### *Kirkland Lake gold deposit*

**Relationships to fault movements:** Gold-bearing veins at Kirkland Lake are hosted by faults cutting through syenite intrusions and Timiskaming stratified rocks. Gold is closely associated with tellurides and, in the central part of the deposit (Wright-Hargreaves, Lake Shore, and Teck-Hughes mines), gold-bearing veins are accompanied by sericitization of the host syenite porphyries. As the veins are fractured and brecciated, they could have formed before faulting (i.e., the faults could have nucleated on veins that occupied older fissures). Alternatively, the veins could have been emplaced during slip along the faults. The available data support the second scenario (i.e., the emplacement of veins at least in part overlapped with fault movements). In brecciated veins, gold and tellurides occur both in quartz fragments and sericite-rich matrix. Occurrence of anhedral telluride grains filling interstices between sericite flakes indicates that tellurides and gold present in the breccia matrix were not released from vein quartz during brecciation but rather were deposited during or shortly after crystallization of sericite. Thus the fault movements that caused vein brecciation occurred during mineralization. The presence of gold and telluride grains along the molybdenite-graphite-coated stylolite bands, which likely represent modified slip surfaces in break veins, further suggests that gold was deposited during slip along the faults.

The sericitic oblique foliation along the Main Break probably formed synchronously with hydrothermal alteration and mineralization. This foliation is interpreted as a shape fabric, which formed during reverse-dextral slip along the fault. This sense of movement is generally consistent with reported offsets of various markers across the deposit: a pipelike syenite body at Macassa, Kirkland Lake Gold, and Teck-Hughes (~450 m, reverse), small quartz-feldspar porphyry intrusions at Lake Shore (400–490 m, reverse), and syenite porphyry-sandstone contact at Toburn mine (~105 m, reverse; Thomson et al., 1950).

Some movements along the ore-hosting faults clearly post-dated mineralization. Postore reactivation of the Main Break and the '04 Break produced striated chloritic slips against which some gold-bearing veins abruptly terminate. Shallowly plunging striations on chloritic slips of the Main Break and '04 Break are probably related to late strike-slip movements that caused sinistral offsets of Matachewan diabase dikes at Teck-Hughes, Lake Shore (25–30 m), Toburn (~2.5 m), and Macassa (~0.75 m; Thompson et al., 1950).

Thomson et al. (1950) interpreted the gently to moderately (20°–50°), south-dipping veins in the hanging wall of the Main Break and '04 Break as extensional veins that formed under the same regional stress field as the steeply dipping (≥60°) fault-fill veins along the Main Break. Although this interpretation has remained largely uncontested over the years, the hanging-wall veins are considerably steeper than the near-horizontal extensional veins typically found in the wall rocks of steep reverse faults in the Abitibi subprovince (e.g., Robert and Poulsen, 2001). They further lack textures that are diagnostic of extensional opening such as fibrous or "stretched crystal" vein infillings (e.g., Ramsay and Huber, 1983, p. 235–257). On the other hand, they are texturally similar to the steep break veins and are commonly associated with minor subsidiary faults (e.g., Fig. 20C) or reactivated preexisting surfaces (e.g., bedding planes and lithologic contacts). Therefore, the hanging-wall veins are interpreted as fault-fill veins that were emplaced in splays of the Main Break and '04 Break.

**Structural timing:** Because the faults cut through largely massive, nonfoliated, syenite intrusions, the relative timing of mineralization and faulting with respect to regional deformation cannot be unequivocally determined. The only regional cleavage in the deposit area is northeast-striking S<sub>4</sub>. Northwest compression during the formation of S<sub>4</sub> and Z-shaped F<sub>4</sub> folds is consistent with reverse-dextral slip along the north-east- to east-northeast-striking ore-controlling faults. It is also consistent with the northwest orientation of stylolitic teeth along northeast-trending stylolite bands that locally host gold and telluride grains in banded break veins. The intramineral phonotephrite dikes provide another possible link between D<sub>4</sub> and the gold-bearing veins. The intramineral timing of the dike emplacement is supported by variably extensive alteration and anomalous gold contents of the dikes and by the presence of quartz vein fragments in them. The dikes exposed on surface are typically foliated by S<sub>4</sub>; however, relationships between dikes and D<sub>4</sub> structures on the outcrop depicted in Figure 27 suggest that emplacement of the dikes, and consequently gold mineralization, was broadly coeval with D<sub>4</sub>.

**Fluid source and genesis:** Genesis of the Kirkland Lake deposit has been discussed by numerous authors, including Watson (1984), Kerrich and Watson (1984), Cameron and Hattori (1987), Robert and Poulsen (1997), and Robert (2003). Watson (1984) and Kerrich and Watson (1984) proposed that the Kirkland Lake deposit was formed from 350° to 460°C fluids of probable crustal metamorphic origin, possibly with an added contribution of magmatic fluids. This was followed by downward penetration of oxidizing, sulfate-bearing, and relatively low temperature (<200° waning to ~50°C) marine or meteoric fluids (Kerrich and Watson, 1984). Cameron and Hattori (1987) presented evidence for oxidized fluids, such as the constant <sup>34</sup>S depletion of sulfides, presence of sulfates in veins and hematite in alteration halos, and proposed a magmatic fluid source related to oxidized felsic magmas. The authors interpreted the syenitic intrusions as "slightly older" than mineralization and suggested that the fluids were likely derived from a deep magma source.

Robert (2001) added a new syenite-associated disseminated gold deposit subgroup to the wider group of intrusion-related gold deposits. The syenite-associated deposits tend to cluster along major faults and comprise variably developed quartz

stockworks in intensely altered (albite and K-feldspar) wall rocks. The deposits are intimately associated with Timiskaming-age monzonitic to syenitic porphyry intrusions near the base of erosional remnants of Timiskaming-type sedimentary rocks. Mineralization was emplaced between 2682 and 2672 Ma (i.e., broadly contemporaneously with Timiskaming sedimentation) and overprinted by regional fabric-forming deformation (Robert, 2001). More recently, Robert (2003) classified the Kirkland Lake deposit as belonging to this subgroup and proposed that the deposit formed prior to regional deformation from fluids derived from alkalic magmas and was overprinted by subsequent deformation.

The interpretations of Cameron and Hattori (1987) and Robert (2003) are consistent with the peculiar geochemical signature of the Kirkland Lake deposit. Kirkland Lake gold veins differ from Upper Canada, Anoki, and McBean mineralization by high Te ( $\text{Te} > \text{Au}$ ), Mo, and low As (Fig. 30). Te is also elevated in the Upper Canada L zone, however Te contents of the L zone are lower than in Kirkland Lake ores, and no gold tellurides, only altaite, have been identified at Upper Canada (Tully, 1963). Other differences include higher As contents and lower Au/Ag ratios at the Upper Canada L zone. The distinctive metal assemblage of the Kirkland Lake high-grade gold veins implies that they formed from fluids that were compositionally distinct and derived from a different source than the gold-mineralizing fluids along the Larder Lake-Cadillac deformation zone and its splays. It is difficult to envision a mechanism that would generate the telluride- and molybdenite-rich mineralization of the Kirkland Lake veins from the same fluid that produced typical low Te-Mo mineralization of the Larder Lake-Cadillac deformation zone gold deposits. Strong correlation of gold and tellurium suggests that they were deposited together, and there was no superposition of discrete gold and tellurium-rich mineralization pulses. The close mineralogical association of native gold and tellurides (Todd, 1928; Thomson et al., 1950) also supports synchronous introduction of gold and tellurium. The possibility that the metal inventory of the Kirkland Lake veins is not fluid source related but instead reflects host-rock signature inherited through fluid-rock interactions at final stages of fluid migration cannot be completely discounted but appears improbable. There is no evidence for volumetrically

significant fluid-wall rock exchange, as the alteration halos directly associated with Kirkland Lake veins are relatively small. Moreover, mineralization is hosted by geochemically variable rocks (e.g., mafic syenite, syenite porphyry, tuff, conglomerate) but no chemical or mineralogical zoning reflecting the host lithologic units has been observed. Thus, most probably, the geochemistry of Kirkland Lake mineralization reflects the fluid chemistry, which was originally different from that of fluids that migrated and deposited gold in the Larder Lake-Cadillac deformation zone and splays. Therefore, we interpret the Kirkland Lake gold deposit to represent a separate hydrothermal system, which is not part of the regional "orogenic" hydrothermal system associated with the Larder Lake-Cadillac deformation zone.

Among the potential fluid sources, derivation of the fluids from alkalic magmas appears most likely. The Kirkland Lake gold deposit shares strong analogies with epithermal-style gold deposits associated with alkaline magmatism. The best known Phanerozoic deposits of this group are the Emperor (Fiji) and Cripple Creek (Colorado) deposits (Jensen and Barton, 2000). Sillitoe (2002) emphasized that giant gold deposits of this class are quite dissimilar to each other as they tend to possess unique sets of geologic characteristics. It is therefore difficult to formulate a simple, universally applicable, set of "diagnostic" empirical criteria for these deposits. Nevertheless, several key geologic parameters of the Kirkland Lake deposit are typical for epithermal-style systems related to alkalic magmatism. These include the following: (1) the localization of the mineralized system in an area of protracted, multistage alkalic magmatism (both volcanic and intrusive) and its spatial association with the alkalic intrusive complex; (2) the occurrence of high-grade (low base metal) veins with high Au/Ag ratios and tellurium contents (e.g.,  $\text{Te} > \text{Au}$  at Kirkland Lake); (3) the presence of gold tellurides and a strong positive gold-tellurium correlation; (4) the common presence of molybdenite; and (5) the occurrence of potassic metasomatism (e.g., local sericitization at Kirkland Lake). Other less pronounced or less well established features of the Kirkland Lake mineralization are also common to alkalic-related epithermal systems, such as locally anomalous vanadium contents and the presence of sulfates, hematite, and possibly magnetite (e.g., Watson and Kerrich, 1984; Cameron and Hattori, 1987).

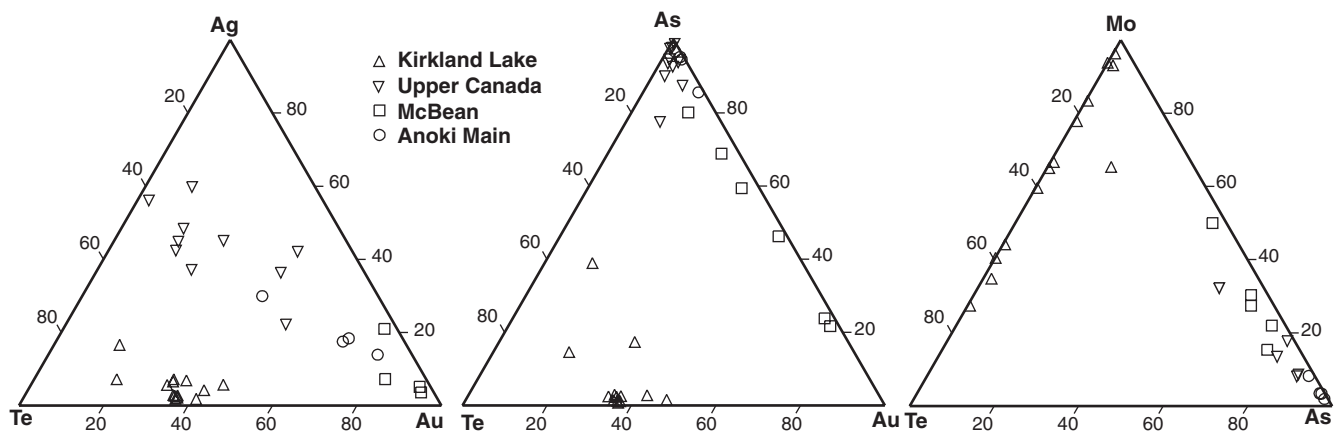


FIG. 30. Comparison of geochemical signatures of Kirkland Lake, Anoki, McBean, and Upper Canada mineralization (data are from Table A2 and Ispolatov et al., 2005).

If the Kirkland Lake mineralization is related to alkalic magmatism, the parent magmatic phase must still be identified. Currently, it is impossible to link the hydrothermal activity to any known igneous phase. The Main Break and subsidiary ore-controlling faults cut and displace the syenite porphyry stock (Hopkins, 1940; Thomson et al., 1950). Mineralization therefore postdates the emplacement and, most probably, the crystallization of the syenite porphyry (i.e., the youngest large-volume alkalic phase exposed at surface). Gold-bearing veins associated with discrete brittle structures extend vertically for at least 2.5 km (e.g., Lake Shore and Wright-Hargreaves mines: Charlewood et al., 1964) within or in close proximity to the stock, and no zoning or textures indicating a transition from melts to gold-bearing fluids (cf. Mustard, 2001) have been reported. Hicks and Hattori (1988) documented that synmineralization hydrothermal alteration overprints the syngenetic alteration of the syenite porphyry. These relationships imply that hydrothermal fluids were not derived from the syenite porphyry intrusion, and thus a deep magmatic source (intrusion or magmatic chamber at depth) is more probable. Whether syenitic intrusions exposed at the present erosional level and mineralizing fluids of the Kirkland Lake gold deposit were derived from a single deep melt reservoir or represent two different magmatic pulses within the Timiskaming-type alkalic magmatic cycle, remains unclear. Due to the inconclusive geochronological data, the time gap between the emplacement of the syenite porphyry stock and mineralization is unknown. Nevertheless, the occurrence of intramineral phonotephrite dikes indicates that the alkalic magmatism overlapped with the hydrothermal activity, and a deep magmatic fluid source is geologically feasible.

### Summary

Three post-Timiskaming fabric-forming deformation events are identified in the Kirkland Lake-Larder Lake gold belt. The earliest fabric-forming event, D<sub>2</sub>, is associated with north-south shortening across the Larder Lake-Cadillac deformation zone and is characterized by the development of a penetrative regional S<sub>2</sub> foliation. D<sub>3</sub> corresponds to an east-west shortening event which locally produced a north-trending S<sub>3</sub> crenulation foliation. D<sub>4</sub> is related to northwest-southeast shortening and is manifested by a regional steep northeast-trending S<sub>4</sub> foliation and Z-shaped F<sub>4</sub> folds.

Gold deposits along the Larder Lake-Cadillac and the Upper Canada deformation zones in the Gauthier mapping area (Upper Canada, Anoki, and McBean deposits) formed synchronously with D<sub>2</sub>. These deposits constitute part of a regional-scale hydrothermal system that corresponds to a ~20-km-long segment of the Larder Lake-Cadillac deformation zone and also includes the Kerr-Addison-Chesterville, Cheminis, and Omega deposits. High-grade veins of the Kirkland Lake gold deposit, associated with the brittle Kirkland Lake fault (Main Break) and the '04 Break, are interpreted to have been emplaced during syn-D<sub>4</sub> reverse-dextral movements on the ore-controlling faults. The distinct metal association (Te > Au, Mo, Pb, Ag, high Au/Ag, low As) of gold-bearing veins suggests that the Kirkland Lake deposit represents a separate hydrothermal system linked to a deep alkalic magmatic fluid source and unrelated to gold mineralization along the Larder Lake-Cadillac and Upper Canada deformation zones.

### Acknowledgments

We thank Queenston Mining Inc. and Kirkland Lake Gold Inc. for granting access to their properties, surface and underground workings, and drill core, and for contributing private geologic data. Kirkland Lake Gold Inc. provided logistical support for underground work of the first author. Geologists Dale Alexander and Frank Ploeger of Queenston Mining Inc., Mike Sutton, Stuart Carmichael, Ken Rattee, Duncan Quick, and Cory Dupuis of Kirkland Lake Gold Inc., and Chris Pegg (consultant) are thanked for their time and sharing their knowledge of geology and gold mineralization of the Kirkland Lake camp and Kirkland Lake-Larder Lake gold belt. We thank *Economic Geology* reviewers Kevin Cassidy and Howard Poulsen and editor Mark Hannington for their comments and suggestions which helped improve the manuscript. The project was supported by the Discover Abitibi Initiative, a regional cluster economic development project based on geoscientific investigations of the western Abitibi greenstone belt. FedNor, Northern Ontario Heritage Fund Corporation, and private sector investors provided the funding for the initiative.

### REFERENCES

- Ayer, J.A., Barr, E., Bleeker, W., Creaser, R.A., Hall, G., Ketchum, J.W.F., Powers, D., Salier, B., Still, A., and Trowell, N.F., 2003, Discover Abitibi. New geochronological results from the Timmins area: Implications for the timing of late-tectonic stratigraphy, magmatism and gold mineralization: Ontario Geological Survey Open File Report 6120, p. 33-1-33-11.
- Ayer, J.A., Trowell, N.F., and Josey, S., 2004, Geological compilation of the Abitibi greenstone belt: Ontario Geological Survey Miscellaneous Release—Data 143.
- Ayer, J.A., Thurston, P.C., Dube, B., Gibson, H.L., Hamilton, M., Hathaway, B., Hocker, S., Houle, M., Hudak, G., Ispolatov, V., Lafrance, B., Leshner, C.M., MacDonald, P.J., Peloquin, A.S., Piercey, S.J., Reed, L.E., and Thompson, P.H., 2005, Overview of results from the greenstone architecture project: Discover Abitibi Initiative: Ontario Geological Survey Open File Report 6154, 146 p.
- Bell, C.C., 1987, Ore petrography, carbonate alteration and geochemistry of the McBean mine, Larder Lake, Ontario: Unpublished B.Sc. thesis, Hamilton, Ontario, McMaster University, 92 p.
- Ben Othman, D., Arndt, N.T., White, W.M., and Jochum, K.P., 1990, Geochemistry and age of Timiskaming alkali volcanics and the Otto syenite stock, Abitibi, Ontario: Canadian Journal of Earth Sciences, v. 27, p. 1304-1311.
- Bleeker, W., Parrish, R.R., and Sager-Kinsman, A., 1999, High-precision U-Pb geochronology of the Late Archean Kidd Creek deposit and Kidd volcanic complex: ECONOMIC GEOLOGY MONOGRAPH 10, p. 43-70.
- Böhlke, J.K., 1988, Carbonate-sulfide equilibria and "stratabound" disseminated epigenetic gold mineralization: A proposal based on examples from Alleghany, California, U.S.A: Applied Geochemistry, v. 3, p. 499-516.
- Cameron, E.M., and Hattori, K., 1987, Archean gold mineralization and oxidized hydrothermal fluids: ECONOMIC GEOLOGY, v. 82, p. 1177-1191.
- Card, K.D., 1990, A review of the Superior province of the Canadian Shield, a product of Archean accretion: Precambrian Research, v. 48, p. 99-156.
- Charlewood, G.H., 1964, Geology of deep developments on the main ore zone at Kirkland Lake: Ontario Department of Mines Geological Circular 11, 49 p.
- Clark, R.J.M., and Bodnar, R., 1987, Gold mineralization associated with Archean stratabound sulphides in the Cheminis deposit near Larder Lake, Ontario: CIM Bulletin 1974, v. 80, p. 45-50.
- Corfu, F., Krogh, T.E., Kwok, Y.Y., and Jensen, L.S., 1989, U-Pb zircon geochronology in the southwestern Abitibi greenstone belt, Superior province: Canadian Journal of Earth Sciences, v. 26, p. 1747-1763.
- Corfu, F., Jackson, S.J., and Sutcliffe, R.H., 1991, U-Pb ages and tectonic significance of Late Archean alkalic magmatism and nonmarine sedimentation, Timiskaming Group, southern Abitibi belt, Ontario: Canadian Journal of Earth Sciences, v. 28, p. 489-503.

- Eisenlohr, B.N., Groves, D., and Partington, G.A., 1989, Crustal-scale shear zones and their significance to Archaean gold mineralization in Western Australia: *Mineralium Deposita*, v. 24, p. 1–8.
- Heffernan, V., 2005, Kirkland Lake: the next Red Lake?: *The Northern Miner*, v. 91, no. 33, p. 1–3.
- Hicks, K.D., and Hattori, K., 1988, Magmatic-hydrothermal and wall rock alteration petrology at the Lake Shore gold deposit, Kirkland Lake, Ontario: Ontario Geological Survey Miscellaneous Paper 140, p. 192–204.
- Hopkins, H., 1940, Faulting at the Wright-Hargreaves mines, with notes on ground movements: *Canadian Institute of Mining and Metallurgy Transactions*, v. 43, p. 685–707.
- Hyde, R.S., 1980, Sedimentary facies in the Archean Timiskaming Group and their tectonic implications, Abitibi greenstone belt, northeastern Ontario, Canada: *Precambrian Research*, v. 12, p. 161–195.
- Irvine, T.N., and Baragar, W.R.A., 1971, A guide to the chemical classification of the common volcanic rocks: *Canadian Journal of Earth Sciences*, v. 8, p. 523–548.
- Ispolatov, V.O., 2005, Precambrian geology of Teck Township transect: Ontario Geological Survey Preliminary Map P.3558, scale 1:10000.
- Ispolatov, V.O., and Lafrance, B., 2005, Precambrian geology of Gauthier Township transect: Ontario Geological Survey Preliminary Map P.3546 revised, scale 1:10000.
- Ispolatov, V., Lafrance, B., Dubé, B., Hamilton, M., and Creaser, R., 2005, Geology, structure, and gold mineralization, Kirkland Lake and Larder Lake areas (Gauthier and Teck Townships): Discover Abitibi Initiative: Ontario Geological Survey Open File Report 6159, 170 p.
- Jackson, S.L., and Fyon, A., 1991, The western Abitibi subprovince in Ontario: Ontario Geological Survey Special Volume 4, Pt. 1, p. 405–482.
- Jaffey, A.H., Flynn, K.F., Glendenin, L.E., Bentley, W.C., and Essling, A.M., 1971, Precision measurements of half-lives and specific activities of  $^{235}\text{U}$  and  $^{238}\text{U}$ : *Physical Review C*, v. 4, p. 1889–1906.
- Jemielita, R.A., Davis, D.W., and Krogh, T.E., 1990, U-Pb evidence for Abitibi gold mineralization postdating greenstone magmatism and metamorphism: *Nature*, v. 346, p. 831–834.
- Jensen, E.P., and Barton, M.D., 2000, Gold deposits related to alkaline magmatism: *Reviews in Economic Geology*, v. 13, p. 279–314.
- Jolly, W.T., 1978, Metamorphic history of the Archean Abitibi belt: *Geological Survey of Canada Paper* 78–10, p. 63–78.
- Kerrick, R., and Watson, G.P., 1984, The Macassa mine Archean lode gold deposit, Kirkland Lake, Ontario: Geology, patterns of alteration, and hydrothermal regimes: *ECONOMIC GEOLOGY*, v. 79, p. 1104–1130.
- Kishida, A., and Kerrich, R., 1987, Hydrothermal alteration zoning and gold concentration at the Kerr-Addison Archean lode gold deposit, Kirkland Lake, Ontario: *ECONOMIC GEOLOGY*, v. 82, p. 649–690.
- Le Bas, M.J., Le Maitre, R.W., Streckeisen, A., and Zanettin, B.A., 1986, Chemical classification of volcanic rocks based on the total alkali-silica diagram: *Journal of Petrology*, v. 27, p. 745–750.
- McCuaig, T.C., and Kerrich, R., 1998, P-T-t-deformation-fluid characteristics of lode gold deposits: Evidence from alteration systematics: *Ore Geology Reviews*, v. 12, p. 381–454.
- Mueller, W., Donaldson, J.A., and Doucet, P., 1994, Volcanic and tectono-plutonic influences on sedimentation in the Archean Kirkland Lake basin, Abitibi greenstone belt, Canada: *Precambrian Research*, v. 68, p. 201–230.
- Mustard, R., 2001, Granite-hosted gold mineralization at Timbarra, northern New South Wales, Australia: *Mineralium Deposita*, v. 36, p. 542–562.
- Phillips, G.N., Groves, D.I., and Martyn, J.E., 1984, An epigenetic origin for Archean banded iron-formation-hosted gold deposits: *ECONOMIC GEOLOGY*, v. 79, p. 162–171.
- Ramsay, J.G., and Huber, M.I., 1983, *The techniques of modern structural geology*, Volume 1: Strain analysis: London, Academic Press, 307 p.
- Robert, F., 1990, Structural setting and control of gold-quartz veins of the Val d'Or area, southeastern Abitibi subprovince: Geology Department (Key Centre) and University Extension, University of Western Australia Short Course Notes 24, p. 167–210.
- 2001, Syenite-associated disseminated gold deposits in the Abitibi greenstone belt, Canada: *Mineralium Deposita*, v. 36, p. 503–516.
- 2003, Giant gold deposits of the Abitibi greenstone belt: WA gold giants and global gold giants [ext. abs.]: University of Western Australia Centre for Global Metallogeny, MSc Short Course, 6–7 February 2003, Extended Abstract Volume, p. 81–90.
- Robert, F., and Poulsen, K.H., 1997, World-class Archaean gold deposits in Canada: An overview: *Australian Journal of Earth Sciences*, v. 44, p. 329–351.
- 2001, Vein formation and deformation in greenstone gold deposits: *Reviews in Economic Geology*, v. 14, p. 111–155.
- Rowins, S.M., Cameron, E.M., Lalonde, A.E., and Ernst, R.E., 1993, Petrogenesis of the Late Archean syenitic Murdock Creek pluton, Kirkland Lake, Ontario: Evidence for an extensional tectonic setting: *Canadian Mineralogist*, v. 31, Pt. 1, p. 219–244.
- Selby, D., and Creaser, R.A., 2004, Macroscale NTIMS and microscale LA-MC-ICP-MS Re-Os isotopic analysis of molybdenite: Testing spatial restrictions for reliable Re-Os age determinations, and implications for the decoupling of Re and Os within molybdenite: *Geochimica et Cosmochimica Acta*, v. 68, p. 3897–3908.
- Sillitoe, R.H., 2002, Some metallogenic features of gold and copper deposits related to alkaline rocks and consequences for exploration: *Mineralium Deposita*, v. 37, p. 4–13.
- Smith, J.P., Spooner, E.T.C., Broughton, D.W., and Ploeger, F.R., 1993, Archean Au-Ag-(W) quartz vein/disseminated mineralisation within the Larder Lake-Cadillac Break, Kerr Addison-Chesterville System, Northeast Ontario, Canada: Ontario Geological Survey Open File Report 5831, 310 p.
- Stein, H.J., Markey, R.J., Morgan, J.W., Hannah, J.L., and Schersten, A., 2001, The remarkable Re-Os chronometer in molybdenite: How and why it works: *Terra Nova*, v. 13, p. 479–486.
- Stevenson, D.B., Broughton, D.W., Cruji, D.R., Masson, M.W., and Parry, S.E., 1995, Geology and exploration history of the amalgamated Kirkland deposit, Kirkland Lake, Ontario: *Exploration and Mining Geology*, v. 4, p. 187–196.
- Still, A.C., 2001, Structural setting and controls of gold mineralization at the Macassa mine, Kirkland Lake, Ontario: Unpublished M.Sc.thesis, Kingston, ON, Queen's University, 151 p.
- Sun, S.S., and McDonough, W.F., 1989, Chemical and isotopic systematics of oceanic basalts: Implications for mantle composition and processes: *Geological Society Special Publication* 42, p. 313–345.
- Thomson, J.E., 1941, Geology of McGarry and McVittie Townships, Larder Lake area: Ontario Department of Mines Annual Report, v. 50, pt. 7, p. 1–99.
- 1945, Township of Teck, District of Timiskaming, Ontario: Ontario Department of Mines Map 1945–1, scale 1:12,000.
- 1950, Geology of Teck Township and the Kenogami Lake area, Kirkland Lake gold belt: Ontario Department of Mines Annual Report, v. 57, pt. 5, p. 1–53.
- Thomson, J.E., and Griffis, A.T., 1941, Geology of Gauthier Township, East Kirkland Lake area: Ontario Department of Mines Annual Report, v. 50, pt. 8, 29 p.
- Thomson, J.E., Charlewood, G.H., Griffin, K., Hawley, J.E., Hopkins, H., MacIntosh, C.G., Ogryzlo, S.P., Perry, O.S., and Ward, W., 1950, Geology of the main ore zone at Kirkland Lake: Ontario Department of Mines Annual Report, v. 57, pt. 5, p. 54–188.
- Todd, E.W., 1928, Kirkland Lake gold area (a detailed study of the Central zone and vicinity): Ontario Department of Mines Annual Report, v. 37, p. 1–176.
- Tully, D.W., 1963, The geology of the Upper Canada mine: *Proceedings of the Geological Association of Canada*, v. 15, p. 61–86.
- Warwick, M., 1981, Gold mineralisation of the flow ores at Kerr Addison mine: Unpublished B.Sc. thesis, London, ON, University of Western Ontario, 101 p.
- Watson, G.P., 1984, Ore types and fluid regimes: Macassa gold mine, Kirkland Lake: Unpublished Ph.D. thesis, London, ON, University of Western Ontario, 341 p.
- Watson, G.P., and Kerrich, R., 1983, Macassa mine, Kirkland Lake: Production history, geology, gold ore types and hydrothermal regimes: Ontario Geological Survey Miscellaneous Paper 110, p. 56–74.
- Wilkinson, L., 1993, Post-Timiskaming structural history of the Larder Lake Cadillac deformation zone, southwestern Abitibi belt, Ontario: Unpublished M.Sc. thesis, Toronto, ON, University of Toronto, 162 p.
- Wilkinson, L., Cruden, A.R., and Krogh, T.E., 1999, Timing and kinematics of post-Timiskaming deformation within the Larder Lake-Cadillac deformation zone, southwest Abitibi greenstone belt, Ontario, Canada: *Canadian Journal of Earth Sciences*, v. 36, p. 627–647.

APPENDIX

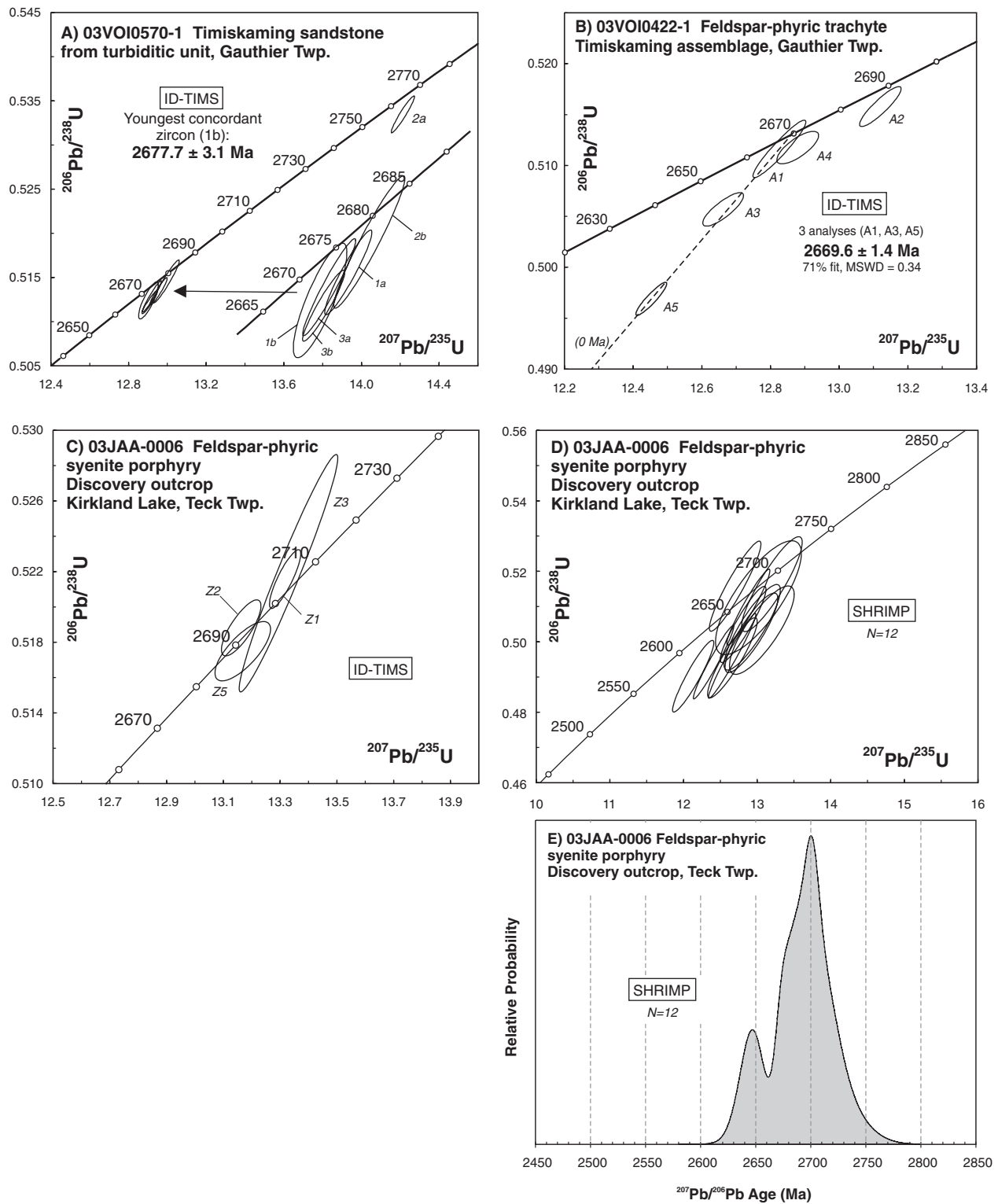


FIG. A1. Results of U-Pb analyses. A, B, C. U-Pb TIMS concordia plots (data are listed in Table A1). D. U-Pb SHRIMP concordia plot. E. Distribution of SHRIMP ages (data are listed in Table A3). Note: In C, imprecise analysis Z4 is omitted for clarity.

TABLE A1. U-Pb (TIMS) Isotope Data (zircon)

Sample Fraction	Analysis no.	Description	Weight (mg)	U (ppm)	Th/U	Pb* (pg)	PbC (pg)	$^{206}\text{Pb}/^{204}\text{Pb}$	$^{206}\text{Pb}/^{238}\text{U} \pm 2\sigma$	$^{207}\text{Pb}/^{235}\text{U} \pm 2\sigma$	$^{207}\text{Pb}/^{206}\text{Pb} \pm 2\sigma$	$^{207}\text{Pb}/^{206}\text{Pb}$ age (Ma)	$\pm 2\sigma$	Disc. (%)	Corr. coeff.			
003VO10570-1; (589218mE, 5331819mN), Sandstone (from turbiditic unit), Timiskaming assemblage, Gauthier Twp.																		
1a	MAH4049	1 clr, med-brn, sharp, subeq euh prism	0.0026	169	0.63	267.1	0.4	35802	0.51336	0.00127	12.9593	0.0357	0.18309	0.00017	2681.0	1.5	0.5	0.9440
1b	MAH4050	1 clr, med-brn, sharp, subeq euh prism	0.0026	122	0.83	193.6	0.4	23858	0.51235	0.00172	12.9073	0.0410	0.18271	0.00034	2677.7	3.1	0.5	0.8370
2a	MAH4051	1 clr, pbr, submd, sl. elong. prism	0.0015	97	0.36	84.6	0.5	9801	0.53342	0.00171	14.2115	0.0459	0.19323	0.00019	2769.8	1.7	0.6	0.9567
2b	MAH4109	1 clr, pbr, submd, sl. elong. prism	0.0007	73	0.47	29.4	0.5	3500	0.51450	0.00199	12.9986	0.0543	0.18324	0.00023	2682.4	2.0	0.3	0.9560
3a	MAH4052	1 large clr, brn, sharp frag	0.0041	145	0.83	368.3	0.6	30646	0.51284	0.00146	12.9239	0.0401	0.18277	0.00016	2678.2	1.5	0.4	0.9581
3b	MAH4110	1 large clr, brn, sharp frag	0.0049	74	0.71	221.0	1.5	8024	0.51216	0.00107	12.9136	0.0322	0.18287	0.00016	2679.1	1.5	0.6	0.9411
03VO10422-1; (587842mE, 5332221mE), Feldspar-phryic trachyte lava, Timiskaming assemblage, Gauthier Twp.																		
A1	MAH4040	1 clr, cls, small, stubby prism	0.0003	107	0.66	16.1	0.4	2359	0.51157	0.00231	12.8293	0.0624	0.18189	0.00030	2670.1	2.8	0.3	0.9401
A2	MAH4041r	1 clr, cls, small, stubby prism	0.0006	74	0.40	27.3	0.8	2114	0.51571	0.00160	13.1224	0.0488	0.18455	0.00031	2694.2	2.8	0.6	0.8938
A3	MAH4042a	1 clr, brn, small, 2:1 prism	0.0003	478	0.53	69.1	2.7	1440	0.50561	0.00135	12.6658	0.0480	0.18169	0.00040	2668.3	3.6	1.4	0.8224
A4	MAH4064a	2 clr, brn, small, 2:1 prism	0.0003	356	0.66	74.8	3.4	1239	0.51170	0.00131	12.8828	0.0499	0.18260	0.00047	2676.6	4.3	0.6	0.7471
A5	MAH4065	2 clr, brn, small, 2:1 prism	0.0003	277	0.69	48.6	0.4	7586	0.49685	0.00134	12.4571	0.0370	0.18184	0.00022	2669.7	2.0	3.2	0.9166
03JAA-0006; (571986mE, 5333892mN), Feldspar-phryic syenite porphyry, Discovery outcrop, Kirdland Lake, Teck Twp.																		
Z1	MAH4014	1 large clr, cls-pbr, frag	0.0043	51	0.65	134.2	4.0	1838	0.52156	0.00135	13.3202	0.0453	0.18523	0.00033	2700.2	2.9	-0.3	0.8614
Z2	MAH4015	1 large clr, cls-pbr, frag	0.0033	70	0.37	134.6	7.8	1021	0.51880	0.00129	13.1645	0.0572	0.18403	0.00052	2689.6	4.7	-0.2	0.7869
Z3	MAH4066	1 small clr, cls-pbr, frag	0.0005	22	0.80	6.6	0.2	1660	0.52193	0.00548	13.3326	0.1426	0.18527	0.00049	2700.6	4.4	-0.3	0.9688
Z4	MAH4016	1 small clr, cls-pbr, subhedra	0.0004	66	0.22	13.0	7.3	125	0.51184	0.00444	12.9887	0.4148	0.18405	0.00456	2689.7	41.3	1.1	0.8674
Z5	MAH4017	1 small clr, cls-pbr, subhedra	0.0007	208	0.46	88.6	8.2	635	0.51748	0.00136	13.1696	0.0802	0.18458	0.00083	2694.4	7.4	0.3	0.7444

Notes: All analyzed fractions represent least magnetic, air-abraded single zircon grains, free of inclusions, cores or cracks, unless otherwise noted; abbreviations: brn = brown, clr = clear, cls = colorless, elong = elongate, eq = equant, euh = euhedral, frag. = fracture(s), frag = fragment, incl = inclusion, pbr = pale brown, prism = prismatic, submd = subrounded, subeq = subequant; Pb\* is total amount (in pg) of radiogenic Pb; PbC is total measured common Pb (in pg) assuming the isotopic composition of laboratory blank;  $^{206}\text{Pb}/^{204}\text{Pb} = 18.221$ ;  $^{207}\text{Pb}/^{204}\text{Pb} = 15.612$ ;  $^{208}\text{Pb}/^{204}\text{Pb} = 39.360$  (errors of 2%); Pb/U atomic ratios are corrected for spike, fractionation, blank, and, where necessary, initial common Pb;  $^{206}\text{Pb}/^{204}\text{Pb}$  is corrected for spike and fractionation; Th/U is model value calculated from radiogenic  $^{208}\text{Pb}/^{206}\text{Pb}$  ratio and  $^{207}\text{Pb}/^{206}\text{Pb}$  age; assuming concordance. Disc. (%) - per cent discordance for the given  $^{207}\text{Pb}/^{206}\text{Pb}$  age; uranium decay constants are from Jaffey et al. (1971); coordinates are UTM zone 17, NAD83



TABLE A3. Ion Microprobe (SHRIMP II) U-Th-Pb Zircon Data

Spot	Struct. dom.	U (ppm)	Th (ppm)	Th/U	Pb* (ppm)	<sup>204</sup> Pb ( <sup>204</sup> Pb)	<sup>206</sup> Pb/ <sup>204</sup> Pb (%)	<sup>207</sup> Pb/ <sup>235</sup> U ± 1s	<sup>206</sup> Pb/ <sup>238</sup> U ± 1s	<sup>207</sup> Pb/ <sup>206</sup> Pb ± 1s	<sup>207</sup> Pb/ <sup>206</sup> Pb ± 1s Age (Ma)	Disc. (%)	Corr. coeff.
03JAA-0006, Feldspar-phyllic syenite porphyry, Discovery outcrop, Kirkland Lake, Teck Township													
10.1	Core	75	30	0.410	43	5	6273	13.0790 ± 0.2901	0.50333 ± 0.00822	0.18846 ± 0.00247	2728.8 ± 21.8	4.5	0.810
12.1	Core	178	92	0.532	101	2	30931	12.7280 ± 0.2140	0.49148 ± 0.00709	0.18782 ± 0.00132	2723.2 ± 11.6	6.5	0.910
9.1	Core	163	100	0.633	96	22	3148	12.9370 ± 0.2371	0.50255 ± 0.00737	0.18670 ± 0.00174	2713.3 ± 15.4	4.0	0.864
4.1	Core	175	84	0.494	101	1	134771	12.9420 ± 0.2522	0.50412 ± 0.00793	0.18620 ± 0.00181	2708.9 ± 16.1	3.5	0.870
2.1	Core	347	208	0.619	199	6	24704	12.4840 ± 0.2555	0.48747 ± 0.00786	0.18574 ± 0.00199	2704.8 ± 17.8	6.5	0.854
13.1	Core	97	33	0.350	55	5	8063	13.2120 ± 0.2725	0.51623 ± 0.00680	0.18562 ± 0.00180	2703.7 ± 16.1	0.9	0.885
5.1	Core?	157	67	0.441	88	2	26889	12.6760 ± 0.2226	0.49559 ± 0.00743	0.18551 ± 0.00139	2702.8 ± 12.4	4.9	0.906
17.1	Core?	273	188	0.710	160	10	11639	12.5840 ± 0.2298	0.49243 ± 0.00779	0.18534 ± 0.00137	2701.3 ± 12.2	5.4	0.917
11.1	Core	619	485	0.809	371	24	10810	12.6740 ± 0.2117	0.49609 ± 0.00785	0.18529 ± 0.00070	2700.8 ± 6.2	4.7	0.975
6.1	Core	345	126	0.376	196	3	44984	13.0320 ± 0.3851	0.51240 ± 0.01055	0.18446 ± 0.00346	2693.4 ± 31.4	1.2	0.776
1.1	Core	256	92	0.372	143	15	7465	12.8220 ± 0.2049	0.50490 ± 0.00705	0.18418 ± 0.00114	2690.9 ± 10.3	2.5	0.923
18.2	Rim	1027	471	0.474	591	7	63052	12.8960 ± 0.1934	0.50977 ± 0.00704	0.18347 ± 0.00080	2684.5 ± 7.2	1.3	0.958
19.1	Core	672	198	0.305	362	16	17928	12.4210 ± 0.1825	0.49430 ± 0.00681	0.18225 ± 0.00067	2673.5 ± 6.1	3.8	0.969
3.1	Magmatic?	492	459	0.965	301	73	2865	12.1440 ± 0.1859	0.49035 ± 0.00664	0.17962 ± 0.00102	2649.4 ± 9.4	3.5	0.931
14.1	Rim	234	55	0.243	129	14	7567	12.7160 ± 0.2316	0.51568 ± 0.00833	0.17884 ± 0.00119	2642.1 ± 11.1	-1.8	0.932

Notes: Uncertainties are reported at 1σ (absolute) and are calculated by numerical propagation of all known sources of error; Pb\* = radiogenic Pb; f<sub>206</sub> (%) = percentage of <sup>206</sup>Pb which is common; disc (%) = percent discordance along a chord to origin for the given <sup>207</sup>Pb/<sup>206</sup>Pb age; corr. coeff. = correlation coefficient (rho)

TABLE A4. Summary of the Re-Os Analytical Data

Sample	Weight (g)	Re (ppm)	$\pm 2\sigma$	$^{187}\text{Os}$ (ppb)	$\pm 2\sigma$	Model age	$\pm 2\sigma$	$\pm 2\sigma$ (incl $\lambda$ )
4744 piece "A" <sup>1</sup>	0.21250	0.544	0.001	15.60	0.03	2677	8	12
4744 piece "A" <sup>1</sup>	0.27619	0.529	0.001	15.09	0.03	2666	8	11
4744 - MS-A <sup>2</sup>	0.02153	0.522	0.001	14.97	0.03	2679	8	11
4744 - MS-B <sup>2</sup>	0.07477	0.574	0.001	16.46	0.03	2678	7	11
Tegren Gracie <sup>3</sup>	0.19986	0.675	0.002	19.50	0.03	2696	7	11
Tegren Gracie <sup>3</sup>	0.27619	0.679	0.002	19.60	0.03	2694	7	11
5030 piece "A" <sup>4</sup>	0.10506	0.714	0.002	22.80	0.04	2976	8	13
5030 piece "A" <sup>4</sup>	0.19309	0.724	0.002	22.75	0.03	2927	8	12
5030 piece "A" <sup>4</sup>	0.32835	0.698	0.002	22.31	0.03	2977	8	12
4247-3 piece "A" <sup>5</sup>	0.04322	0.765	0.002	22.74	0.03	2773	7	11
4247-3 piece "B" <sup>6</sup>	0.05351	0.900	0.002	26.11	0.04	2710	7	11

<sup>1</sup>Fractions of a single drilled mineral separate of 0.50 g

<sup>2</sup>Aliquants from a bulk mineral separate

<sup>3</sup>Fractions of a single drilled mineral separate of 0.48 g

<sup>4</sup>Fractions of a single drilled mineral separate of 0.71 g

<sup>5,6</sup> Concentrates derived from two separate rock fragments

